# Effects of Obstacle Geometry on Jet Mixing for Releases of Silane

By C. F. Sposato, W. J. Rogers, and M. S. Mannan
Mary Kay O'Connor Process Safety Center
Department of Chemical Engineering
Texas A & M University
College Station, TX 77843

## Abstract

Releases of silane into air and the effects of obstacles were modeled with the Computational Fluid Dynamics (CFD) code, FLUENT. First the CFD code simulated the release of a free turbulent jet of silane into air to assure that the code agreed with established trends for turbulent jets. Then FLUENT was used to model the flow of silane when confined due to a wall, or impinged by an obstacle such as a flat plate. Computer simulated concentration profiles of a silane air mixture were analyzed to determine mixture volumes between the mixture explosive limits. From each volume of an explosive mixture, the masses of silane and air were determined. The volume of the flammable mixture and the amount of silane within the flammable mixture were determined as functions of plate radius and plate distance. The volumes decrease if the plate is close to nozzle where the radial contribution dominates, and the volumes increase with increasing plate distance where the axial contribution dominates. The volumes increase, decrease, or remain constant depending on the plate diameter.

## Background

Silane is a pyrophoric gas primarily used in the semiconductor industry for Chemical Vapor Deposition (CVD) of thin dielectric films on substrates. Silicon dioxide films form by reacting silane with an oxidizer. Silane is also used in the manufacture of ICs and photovoltaic cells. Uses of silane can potentially present fire and explosion hazards because of its pyrophoric nature (4, 11).

In 1994 AT&T Bell Laboratories and SEMATECH surveyed various industries that use silane like semiconductor, solar cell, and flat panel display manufacturers and universities. Out of the 55 incident surveys returned, 38 of them reported an unplanned silane release during the last five years. Fire was often the consequence of a silane release. Injuries in the incident surveys included one serious burn, one minor burn, and one temporary hearing loss. Most of the silane incidents, 45%, occurred during processing, 21% during maintenance, and 21% during cylinder changes (11).

Silane is a pyrophoric gas because its autoignition temperature in air, which has been as low as $-100^0$C, is below the ambient temperature (4). Because it is pyrophoric, silane can spontaneously ignite if it is exposed to the air. For silane-air mixtures less than or equal to 30 mole% silane the stoichiometric combustion reaction of silane in air is as follows:

$$SiH_4 + 2O_2 + N_2 \rightarrow SiO_2\,(s) + 2H_2O + N_2$$

When silane is 70 mole% or greater silane reacts with oxygen as follows:

$$SiH_4 + O_2 + N_2 \rightarrow SiO_2\,(s) + 2H_2 + N_2$$

For mixtures between 30 mole% and 70 mole%, both reactions take place (6).

Even though silane is pyrophoric it may not always ignite immediately when exposed to oxygen. When released it may not ignite depending on factors such as release velocity, pressure, temperature, humidity, presence of turbulence, and release geometry such as the cross sectional area of release (6). There are five known ignition types of silane: prompt ignition, ignition during flow decay, ignition at shutoff, piloted ignition, and bulk autoignition. Prompt ignition occurs when the reaction starts at the beginning of a silane release. If the silane does not ignite promptly, then a silane/air mixture forms. Ignition during flow decay occurs when the flow of silane is gradually decreased. There is only minimal pressure development from this type of release. Ignition at shutoff occurs when the flow of silane is suddenly stopped. The possibility for this type of ignition is very likely. Pressure development from the reaction can be high, because an explosive volume can form for concentrations between the explosive limits. Piloted ignition occurs when the silane/air mixture is ignited from an external ignition source (13). From experiments igniting stable silane/air mixtures from an external source, the lower explosive limit (LEL) was determined to be around 1.4 volume% of silane and the upper explosive limit (UEL) was determined to be around 96 volume% (14). Bulk autoignition is similar to piloted ignition, but an external ignition source is not needed (13).

## Previous Research

Some research has studied the ignition characteristics of silane. The bulk of testing and research was performed by Hazards Research Corporation (HRC) in the late 1970s and early 1980s, Union Carbide in the late 1980's and early 1990's, and Factory Mutual Research Corporation (FMRC) in the mid 1990's. The Compressed Gas Association (CGA) is currently performing tests on silane releases.

HRC conducted test with releases of silane into the air through ¼, ½, and ¾ inch diameter tubes. These tests were conducted at initial line pressures of 50, 100, and 500 psig for the ½ and ¾ inch diameter tubes. For the ¼ inch tube, tests were only conducted at 500 psig. Prompt ignition was not observed at initial pressures of 100 and 500 psig but was observed at 50 psig for the ¾ inch tubes (7,8).

At Union Carbide, Britton presented data that show the effects of sudden releases of silane into air. Britton concluded that the probability of ignition of a released silane jet decreases with increased flow velocity and decreased temperature. Therefore, autoignition of the jet seems to take place if the exit velocity is below a critical value. The critical velocity depends on factors such as the diameter of the orifice, temperature of the jet and the surrounding environment, and the release geometries. Britton reported critical velocities in the range of 10 – 20 m/s at an ambient temperature of 32$^{o}$F and 50 m/s at a temperature of 43$^{o}$F for a release from a ½ inch tube (4).

FMRC studied the ignition characteristics of releases of 100% silane and the effects of leak size and geometry on releases of 100% silane. First they simulated an accidental release of silane into a ventilated cabinet from a regulated pressure line of a ¼ inch OD tube (0.18 inch ID) at pressures ranging from 30 to 300 psig. For an exit line of a ¼ inch OD, prompt ignition was very likely with a release pressure below 70 psig. For line pressures between 100 psig and 300 psig, prompt ignition probability was about 50/50. Ignitions were observed when the flow of silane was terminated (14, 15).

FMRC also studied the effects of leak size and geometry on releases of 100% silane. The effect of leak size was studied by releasing silane from a regulated pressure line (8 – 100 psig) by varying the diameter of the discharge line. These tests were conducted by releasing silane from a 1/8 inch tube (instead of a ¼ inch tube). Only one of the twelve tests (at a pressure of 33 psig) ignited promptly. The silane did not ignite promptly even at a line pressure as low as 7.8 psig from a 1/8 inch tube while it ignited around 70 psig for a ¼ inch line. The results of these tests were quite surprising and unexpected because the silane would not ignite for even very low line pressures from a 1/8 inch. Ignitions were observed at flow shutoff or flow decay. Leak size certainly does seem to be factor for a delayed ignition. Tests were carried out also when the release from a ¼ inch line was aimed at a flat plate. The plate is supposed to simulate an object like a cabinet or a wall close to a leak. For a release from a ¼ inch diameter exit line aimed at a flat plate, prompt ignitions were always observed for line pressures below 130 psig. At higher pressures, the split between cases of prompt and delayed ignition was about 50/50 (15).

## Present Research at Texas A & M University

Present research is focused on releases of silane that ignite when the flow of silane is shut off. The goal of the research is to determine the amount of silane that forms an explosive mixture with air before the mixture ignites. The research is concerned only with the mixture that forms before a reaction and not during or after a reaction. Determining the amount of the silane involved in a reaction (concentrations above the LEL) can help determine the pressure development resulting from the mixture ignition. This will include studying the effects of plate impingement (to simulate a release blocked by a wall or cabinet) on the amount of silane involved and the volume occupied by the explosive mixture – the volume between the UEL and LEL. The ultimate goal is to develop generalized correlations to determine the total mixture volume and amount of silane within the volume at any plate distance with any plate radius.

Instead of conducting laboratory experiments to determine the effects of obstacles on the explosive volume and amount of silane in the explosive volume, the Computational Fluid Dynamics (CFD) code FLUENT is used to simulate the release of silane and the effects obstacles have on the release. There are several reasons to use CFD code to approximate this system instead of running a laboratory experiment. Because silane forms a flammable mixture with air and can ignite at ambient conditions, it would be difficult to estimate the amount of mass involved in the explosive mixture even if the mixture ignites when the flow is shutoff. In addition, it might be difficult to determine how much mass was initially present that forms an explosive mixture before it ignites. With CFD code, one does not have to risk forming an explosive mixture or have unaccounted mass. CFD code

would be safer to use for this system since one does not have to be concerned about flammable chemicals and mixtures. Also it is less costly to use CFD code then buying lab equipment and flammable chemicals.

FLUENT was specifically chosen to simulate this scenario. FLUENT can readily calculate concentrations and the volume between concentrations, which can be used to determine the mass involved in ignition for axisymmetric and turbulent systems.

# Free Jet

## Problem Description

The first problem modeled with FLUENT was a round turbulent free jet of silane. The term free means that the jet is unconfined. Much research has already been done on turbulent free jets and analyzing concentration profiles along the jet axis (1, 5). The volume between the explosive limits and the amount of silane within the explosive volume has already been determined (15). The purpose of running a simulation on a free jet of silane is to validate FLUENT's prediction for the mean mixture fraction for a turbulent jet and its prediction for the total volume and the amount of silane in the total volume.

Figure 1 shows the geometry of the problem. The inner diameter of the nozzle is 0.18 inches (4.6 mm). Because the jet is released into a relatively infinite environment, the computational domain must approximate an infinite domain, and must be large enough to contain the entire explosive volume, but not too large to lose accuracy. The length of the computational domain to simulate the atmosphere is 2 m, and the diameter of the computational domain is 0.5 m. FLUENT uses the boundary condition type of a pressure inlet to represent an unconfined boundary. A gauge pressure must be entered for a pressure inlet so a gauge pressure of zero is entered to model the atmosphere. Because the jet is round, and therefore axisymmetric, only the upper half of Figure 1 is modeled with CFD code.

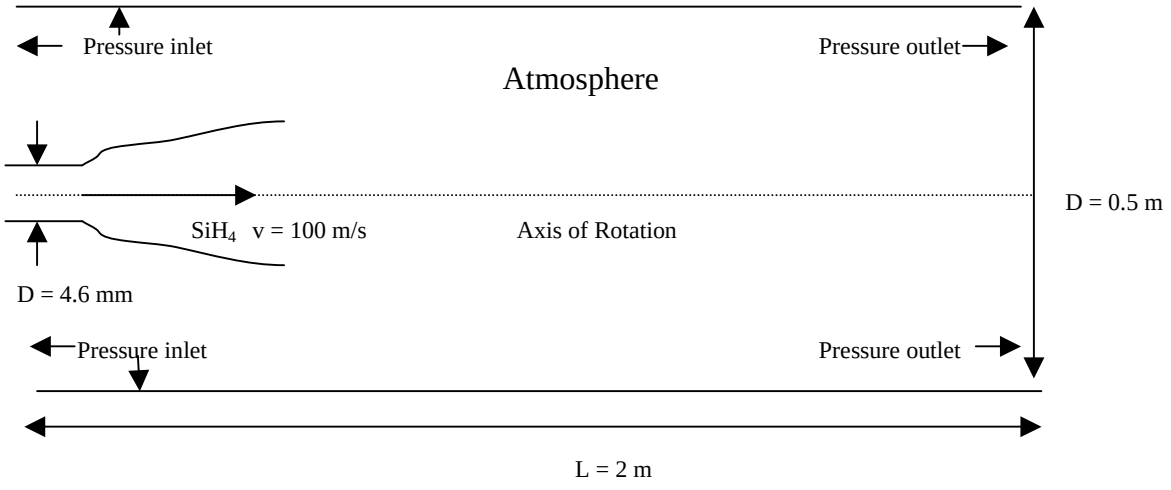


Figure 1: Problem Description for a Free Jet

**Fluid Properties**

FLUENT contains a database of compounds, and the fluid properties for silane and air are taken from the database and are listed in Table 1. Physical properties for the mixture are calculated with equations available in FLUENT. The density of the air/mixture is defined with the ideal-gas mixing law:

$$\rho = \frac{P_{op}}{RT\Sigma_i \frac{m_i}{M_i}} \tag{1}$$

where R is the universal gas constant, $m_i$ is the mass fraction of species i, $M_i$ is the molecular weight of species i, and $P_{op}$ is the operating pressure (atmospheric pressure). The mixture properties of viscosity, mass diffusivity, and operating pressure are taken as constant and again are taken from the FLUENT database of compounds. Using constant molecular transport properties is acceptable because the flow is turbulent. The molecular transport properties play a minor role compared to turbulent transport (9). Physical properties calculated for the mixture and used by FLUENT are listed in Table 2.

Table 1: Physical Properties of Air and $SiH_4$

| | Air | $SiH_4$ |
|---|---|---|
| Molecular Weight (kg/kgmol) | 28.966 | 32.11788 |
| Density, $\rho$ ($kg/m^3$) | 1.225 | 1.308 |
| Viscosity, $\mu$ (kg/m-s) | $1.7894*10^{-5}$ | $1.09*10^{-5}$ |
| Temperature, T (K) | 300 | 300 |

Table 2: Physical Properties of Mixture

| | |
|---|---|
| Viscosity, $\mu$ (kg/m-s) | $1.72*10^{-5}$ |
| Mass Diffusivity, $D_{ij}$ ($m^2/s$) | $2.88*10^{-5}$ |
| Operating Pressure, $P_{op}$ (Pa) | 101,325 |
| Temperature (K) | 300 |

**Boundary Conditions**

Boundary conditions for the jet exit and the air flow must be entered into FLUENT. The boundary type for the jet was set as a velocity inlet. The axial velocity from the silane jet is specified as 100 m/s with a silane mass fraction of 1.0. The Reynolds number based on the jet nozzle's inner diameter is approximately 55,000. The turbulent parameters of turbulence intensity, I, and hydraulic diameter, $D_H$ were specified to approximate turbulence. The FLUENT User's Guide recommends the following equation for fully developed pipe flow:

$$I \cong 0.16(\mathrm{Re}_{D_H})^{-1/8} \tag{2}$$

The above equation was used to approximate the turbulence intensity for the jet. With a Reynolds number of 55,000, turbulence intensity approximately equals 4% (9).

The boundary type for air is set as a pressure inlet with zero gauge pressure and a silane mass fraction of 0. Turbulence parameters must also be specified for a boundary type of pressure inlet. The FLUENT manual recommends using a turbulence intensity and viscosity ratio for an external flow boundary type. The viscosity ratio is defined as the ratio of turbulent viscosity to laminar viscosity, $\mu_t/\mu$. Since the flow at the pressure inlet is not very turbulent, very low turbulence parameters are used. A viscosity ratio of 1 and a turbulence intensity of 0.5% were specified. Table 3 summarizes the inlet boundary conditions (9).

Table 3: Inlet Boundary Conditions

| | Air | $SiH_4$ |
|---|---|---|
| Velocity, v, (m/s) | N/A | 100 |
| Gauge Pressure, $P_g$ (Pa) | 0 | N/A |
| Temperature, T (K) | 300 | 300 |
| Turbulence Intensity, I (%) | 0.5 | 4.0 |
| Hydraulic Diameter, $D_H$ (m) | N/A | 0.0046 |
| Viscosity Ratio, $\mu_t/\mu$ | 1.0 | N/A |
| Mass Fraction of $SiH_4$ | 0 | 1.0 |

**Grid**

The upper half of Figure 1 was modeled with a quadrilateral mesh. Weighting factors were used to concentrate the grid at the symmetry axis and near the jet exit. This ensures that the regions with large gradients in velocity and concentration are accurately predicted. Also, the areas with dense mesh were positioned where most of jet flow took place. Figure 2 shows the full grid, and Figure 3 shows a close up of the grid around the nozzle and jet exit.

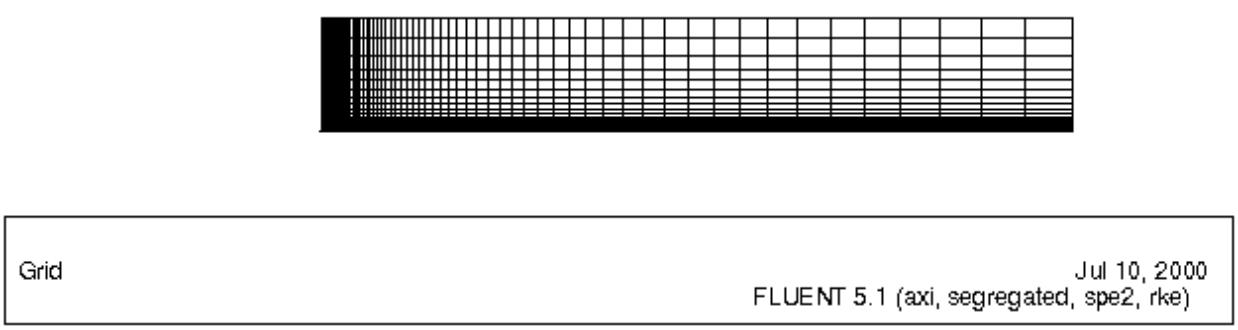


Figure 2: Full Grid for a Free Jet

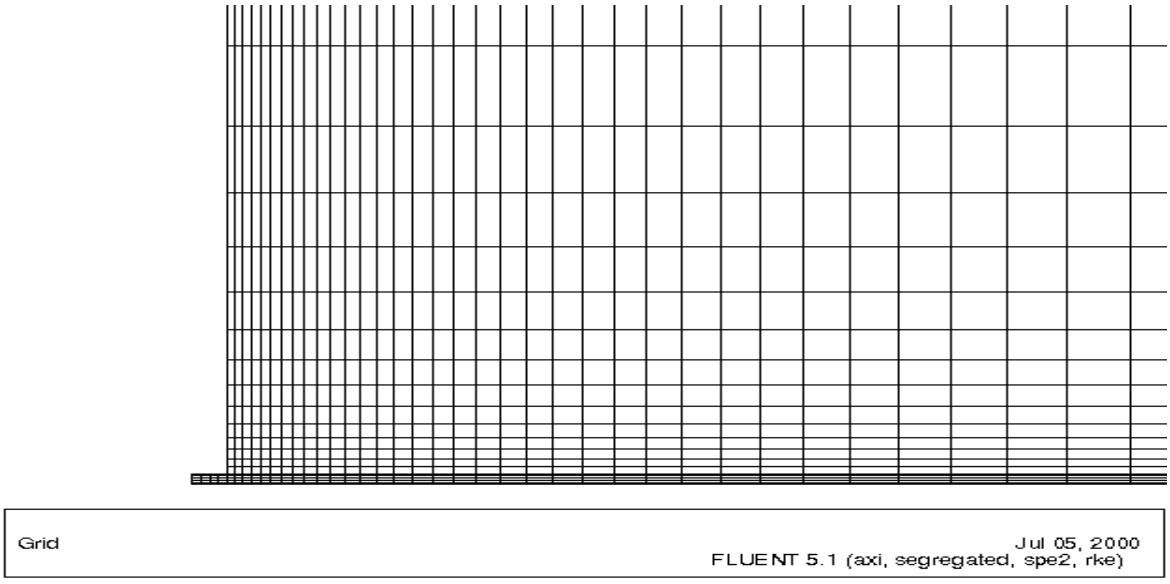


Figure 3: Close up of the Grid for a Free Jet

**Mathematical Basis**

FLUENT solves the conservation of mass and momentum equations. Because this problem is turbulent and also requires multiple species mixing, FLUENT also solves a species conservation equation and two additional transport equations for turbulence. All the transport equations are discretized into algebraic equations and solved by iteration in the finite cells of the grid.

The equation for the conservation of mass, or the continuity equation, can be written for steady state 2D axisymmetric geometry as follows:

$$\frac{\partial(\rho u)}{\partial x}+\frac{\partial(\rho v)}{\partial r}+\frac{\rho v}{r}=0 \tag{3}$$

where x is the axial coordinate, r is the radial coordinate, u is the axial velocity, and v is the radial velocity.

For steady state 2D axisymmetric flow, the conservation of momentum equations, or the Navier-Stokes equations in the axial and radial direction, are written as follows:

$$\frac{1}{r}\frac{\partial(r\rho uu)}{\partial x}+\frac{1}{r}\frac{\partial(r\rho vu)}{\partial r}=-\frac{\partial p}{\partial x}-\frac{1}{r}\frac{\partial(r\tau_{rx})}{\partial r}-\frac{\partial\tau_{xx}}{\partial x} \tag{4}$$

$$\frac{1}{r}\frac{\partial(r\rho uv)}{\partial x}+\frac{1}{r}\frac{\partial(r\rho vv)}{\partial r}=-\frac{\partial p}{\partial r}-\frac{1}{r}\frac{\partial(r\tau_{rr})}{\partial r}-\frac{\partial\tau_{rx}}{\partial x}+\frac{\tau_{\theta\theta}}{r} \tag{5}$$

where p is the static pressure and $\tau_{ij}$ is the stress tensor. The stress tensors are defined as (9, 3)

$$\tau_{rx}=-\mu\left[\frac{\partial u}{\partial r}+\frac{\partial v}{\partial x}\right] \tag{6}$$

$$\tau_{xx}=-\mu\left[2\frac{\partial u}{\partial x}-\frac{2}{3}(\nabla\cdot v)\right] \tag{7}$$

$$\tau_{rr}=-\mu\left[2\frac{\partial v}{\partial r}-\frac{2}{3}(\nabla\cdot v)\right] \tag{8}$$

$$\tau_{\theta\theta}=-\mu\left[2\frac{v}{r}-\frac{2}{3}(\nabla\cdot v)\right] \tag{9}$$

and

$$\nabla \cdot v = \frac{\partial u}{\partial x} + \frac{\partial v}{\partial r} + \frac{v}{r} \tag{10}$$

For species transport, conservation equation must be solved for each chemical species. FLUENT solves the local mass fraction of each species, $m_{i'}$, with a convection-diffusion equation for the i'th species. The species conservation equation for the i'th species is described as follows

$$\frac{\partial(\rho u_i m_{i'})}{\partial x_i} = -\frac{\partial J_{i',i}}{\partial x_i} \tag{11}$$

where $J_{i',i}$ is the diffusion flux of species i', which arises from concentration gradients and is defined as (9)

$$J_{i',i} = -\rho D_{i',m} \frac{\partial m_{i'}}{\partial x_i} \tag{12}$$

However, Equations 4 through 12 are for low Reynolds flow. The Reynold's number based on the jet diameter was around 55,000. Therefore, the flow is turbulent and must be modeled with turbulence models. Two turbulence models, the standard k-ε model and the realizable k-ε model, were used to simulate turbulent free jets.

Turbulence is the unsteady, aperiodic motion in which the velocity components fluctuate. To model turbulence, the velocity is decomposed into the mean and fluctuating terms:

$$U_i(t) \equiv U_i + u_i(t) \tag{13}$$

where $U_i(t)$ is the velocity, $U_i$ is the mean velocity and $u_i(t)$ is the fluctuating velocity. Similar definitions exist for pressure and species concentrations (9).

Instead of solving the standard Navier-Stokes equations for turbulent flow, the Reynolds Averaged Navier-Stokes equations are solved. The Reynolds Averaged Navier-Stokes equation in steady state form (and Cartesian coordinates) is written as

$$\rho U_k \frac{\partial U_i}{\partial x_k} = -\frac{\partial p}{\partial x_i} + \mu \frac{\partial^2 U_i}{\partial x_j \partial x_j} + \frac{\partial R_{ij}}{\partial x_j} \tag{14}$$

where $R_{ij}$ are the Reynolds stresses (fluctuations) and are defined as follows (9):

$$R_{ij} = -\rho \overline{u'_i u'_j} \tag{15}$$

Introducing the Reynolds stresses introduces more unknowns so the set of equations must be closed. The Boussinesq hypothesis relates the Reynolds stresses to the mean velocity gradients (9):

$$-\rho\overline{u'_i}\overline{u'_j} = \mu_t\left(\frac{\partial u_i}{\partial x_j}+\frac{\partial u_j}{\partial x_i}\right)-\frac{2}{3}\left(\rho k+\mu_t\frac{\partial u_i}{\partial x_i}\right)\delta_{ij} \tag{16}$$

For both k-ε models two more transport equations, the turbulent kinetic energy, k, and the turbulence dissipation rate, ε are introduced. The turbulent viscosity, $\mu_t$, is a function of k and ε. The k and ε are solved so that turbulent viscosity can be computed for the Reynolds Averaged Navier-Stokes equation and close the set of equations.

$$k \equiv \frac{\overline{u_i u_i}}{2} \tag{17}$$

$$\varepsilon \equiv \nu\frac{\partial u_i}{\partial x_j}\left(\frac{\partial u_i}{\partial x_j}+\frac{\partial u_j}{\partial x_i}\right) \tag{18}$$

$$\mu_t \equiv \rho C_\mu\frac{k^2}{\varepsilon} \tag{19}$$

The k-ε turbulence model is a semi-empirical model. It assumes that the flow is fully turbulent, and the effects of molecular viscosity are negligible. The transport equation for the turbulent kinetic energy is the same for the standard k-ε model and the realizable k-ε model, and it is defined from the following transport equation:

$$\rho U_i\frac{\partial k}{\partial x_i} = \mu_t\left(\frac{\partial U_j}{\partial x_i}+\frac{\partial U_i}{\partial x_j}\right)\frac{\partial U_j}{\partial x_i}+\frac{\partial}{\partial x_i}\left\{\mu+\left(\frac{\mu_t}{\sigma_k}\right)\frac{\partial k}{\partial x_i}\right\}-\rho\varepsilon \tag{20}$$

The left hand side of the equation represents convection. The first term on the right hand side models the generation of turbulent kinetic energy due to mean velocity gradients. The middle term represents diffusion, and the last term is the destruction of kinetic energy (9). $\sigma_k$ is the turbulent Prandtl number for k. The default value of $\sigma_k$ was used, and it was originally determined from experiments and is generally accepted for a wide range of flows. All model constants for both turbulence models are listed in Table 4.

The transport equation for the turbulent dissipation for the standard k-ε model is given as follows:

$$\rho U_i \frac{\partial \varepsilon}{\partial x_i} = C_{1\varepsilon}\left(\frac{\varepsilon}{k}\right)\mu_t\left(\frac{\partial U_j}{\partial x_i}+\frac{\partial U_i}{\partial x_j}\right)\frac{\partial U_j}{\partial x_i}+\frac{\partial}{\partial x_i}\left\{\left(\mu_t/\sigma_\varepsilon\right)\frac{\partial \varepsilon}{\partial x_i}\right\}-C_{2\varepsilon}\left(\frac{\varepsilon^2}{k}\right) \tag{21}$$

The left hand side of the equation represents convection. The first term on the right hand models generation of turbulent kinetic energy. The middle term again represents diffusion, and the last term models destruction. Again, $\sigma_\varepsilon$, $C_{1\varepsilon}$, and $C_{2\varepsilon}$ are empirical constants for the model, and they are listed in Table 4.

The standard k-ε model is the most common model used in industry. However, the k-ε model has one major weakness. It predicts planar jets fairly accurately, but it does not predict round jets accurately. To correct the "round jet anomaly" the dissipation transport equation in the realizable k-ε model was modified to predict axisymmetric jets more accurately. The realizable k-ε turbulence is realizable because it ensures that the normal stresses are always positive, $u_i^2>0$, so it satisfies mathematical constraints. Therefore, there are two main differences between the standard and realizable k-ε models. The transport equation for the turbulent dissipation is derived differently for each model, and $C_\mu$ in the equation for turbulent viscosity is allowed to vary in the realizable model (9). The alternate form of the turbulent viscosity is defined as:

$$\mu_t \equiv \rho C_\mu \frac{k^2}{\varepsilon} \tag{22}$$

where $C_\mu$ is now allowed to vary according to the following equation:

$$C_\mu = \frac{1}{A_0 + A_s \dfrac{U^* k}{\varepsilon}} \tag{23}$$

$A_0$, $A_s$ and $U^*$ are function of velocity gradients. They are defined as

$$U^* \equiv \sqrt{S_{ij}S_{ij}+\tilde{\Omega}_{ij}\tilde{\Omega}_{ij}} \tag{24}$$

$$\tilde{\Omega}_{ij} = \Omega_{ij} - 2\in_{ijk}\omega_k \tag{25}$$

$$\Omega_{ij} = \overline{\Omega_{ij}} - \in_{ijk}\omega_k \tag{26}$$

$\overline{\Omega_{ij}}$ is the mean rate-of-rotation tensor with angular velocity $\omega_k$. The constants $A_0$ and $A_s$ are defined as follows

$$A_0 = 4.04 \tag{27}$$

$$A_s = \sqrt{6}\cos\phi \tag{28}$$

where

$$\phi = \frac{1}{3}\arccos(\sqrt{6}W) \tag{29}$$

$$W = \frac{S_{ij}S_{jk}S_{ki}}{\tilde{S}} \tag{30}$$

$$\tilde{S} = \sqrt{S_{ij}S_{ij}} \tag{31}$$

$$S_{ij} = \frac{1}{2}\left(\frac{\partial u_j}{\partial x_i} + \frac{\partial u_i}{\partial x_j}\right) \tag{32}$$

The modified transport equation for the turbulent dissipation for the realizable k-ε model is

$$\rho U_i \frac{\partial \varepsilon}{\partial x_i} = \rho C_1 S\varepsilon + \frac{\partial}{\partial x_j}\left\{\left(\mu + \frac{\mu_t}{\sigma_\varepsilon}\right)\frac{\partial \varepsilon}{\partial x_{ji}}\right\} - \rho C_2 \frac{\varepsilon^2}{k + \sqrt{\nu\varepsilon}} \tag{33}$$

$$C_1 = \max\left[0.43, \frac{\eta}{\eta + 5}\right] \tag{34}$$

$$S \equiv \sqrt{2S_{ij}S_{ij}} \tag{35}$$

and

$$\eta = Sk/\varepsilon \tag{36}$$

Although the terms are different, they model the same physical features as the standard k-ε model. The left hand side models convection, the first term on the right hand side models generation, the middle terms represents diffusion, and the last term is the destruction term. All the turbulence model constants are defined in Table 4 (9).

Table 4: Turbulence Parameters for the Standard and Realizable k-ε Models

| | Standard Model | Realizable Model |
|---|---|---|
| $C_\mu$ | 0.09 | varies |
| $\sigma_k$ | 1.0 | 1.0 |
| $\sigma_\varepsilon$ | 1.3 | 1.2 |
| $C_{1\varepsilon}$ | 1.44 | 1.44 |
| $C_{2\varepsilon}$ | 1.92 | N/A |
| $C_2$ | N/A | 1.9 |

FLUENT requires turbulence parameters to be specified at the inlet and outlet boundary types. The k and ε can be specified explicitly; or more convenient quantities like turbulent intensity, turbulent viscosity ratio, or turbulence length scale can be specified to estimate k and ε (9).

The turbulence intensity, I, is defined as the ratio of the root-mean-square of the velocity fluctuations, u', to the mean flow velocity, $u_{avg}$.

$$I = \frac{u'}{\bar{u}} \tag{37}$$

The FLUENT manual recommended Equation 2 to estimate intensity for fully developed pipe flow. Equation (38) relates turbulent intensity to turbulent kinetic energy:

$$k = \frac{3}{2}(u_{avg} I)^2 \tag{38}$$

The physical quantity, turbulence length scale, $\ell$, is related to the large eddies in turbulent flow. Turbulence length scale is limited to the size of the duct. For the nozzle, the hydraulic diameter was specified to estimate the turbulence length scale. Turbulence length scale determines turbulent dissipation, ε, from the following equation:

$$\varepsilon = C_{\mu}^{3/4} \frac{k^{\frac{3}{2}}}{\ell} \tag{39}$$

For the external boundary conditions, the turbulent viscosity ratio, $\mu_t/\mu$, was specified. The ε can be derived from the turbulent viscosity ratio from

$$\varepsilon = \rho C_{\mu} \frac{k^2}{\mu} \left( \frac{\mu_t}{\mu} \right)^{-1} \tag{40}$$

The equation for the diffusion flux of species i, Equation 12, must also be corrected for turbulent flows as follows (9):

$$J_{i',i} = -\left( \rho D_{i',m} + \frac{\mu_t}{Sc_t} \right) \frac{\partial m_{i'}}{\partial x_i} \tag{41}$$

where $Sc_t$ is the turbulent Schmidt number

$$Sc_t = \frac{\mu_t}{\rho D_t} \tag{42}$$

**Results**

Figure 4 shows the upper profile of the explosive volume (volume between 1.4 volume% and 96 volume%) created by a free jet of silane released into air. Because the jet is axisymmetric, the area in the figure is rotated around the jet axis; and the resulting volume is the explosive volume. Very close to the nozzle the concentrations of silane are very high. As the jet entrains air from the atmosphere the jet of silane becomes diluted. The silane concentration decreases as the distance from the nozzle increases. Figure 5 shows the velocity vectors, and the entrainment of air into the high-velocity silane jet is clearly visible in this figure.

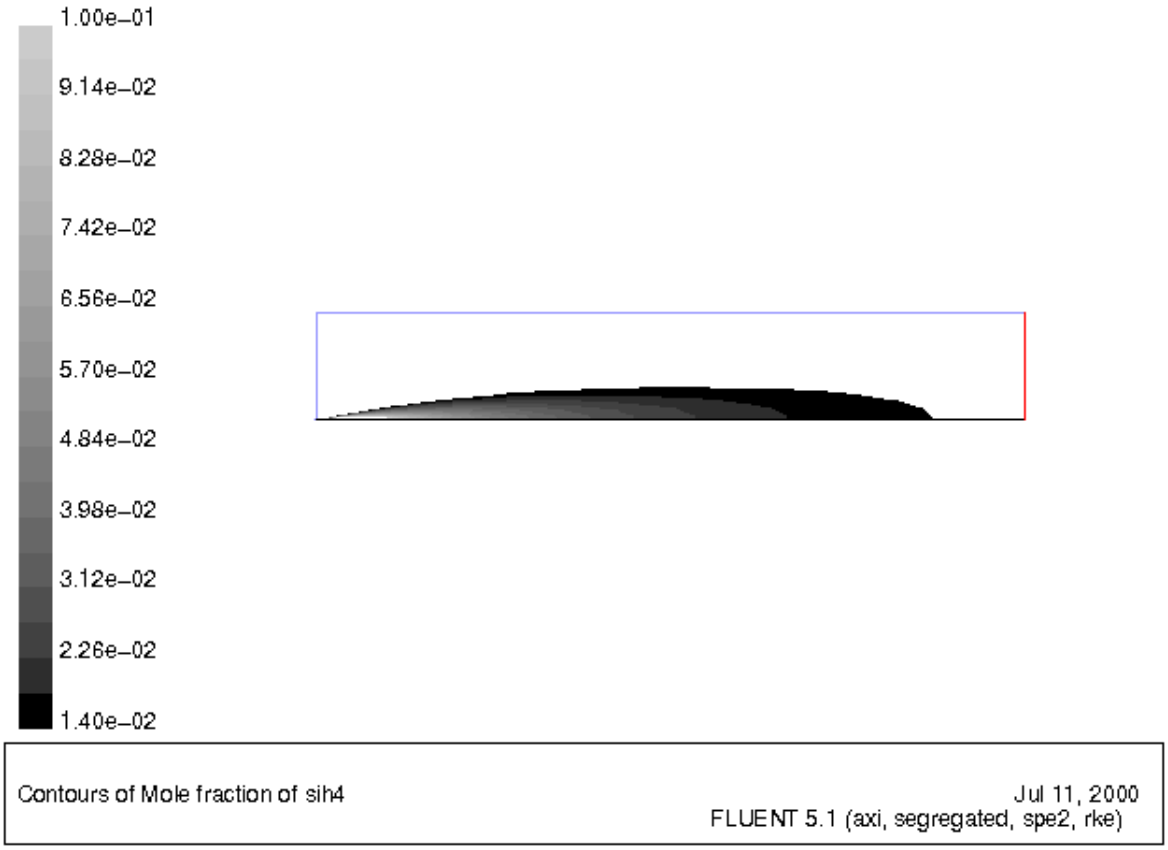


Figure 4: Profile of Explosive Volume for a Free Jet of Silane for the Realizable k-ε Model (the upper concentration was clipped to 0.10 to see the resolution better in the bulk of the jet, but the actual upper concentration limit should be 0.96 mole fraction of silane)

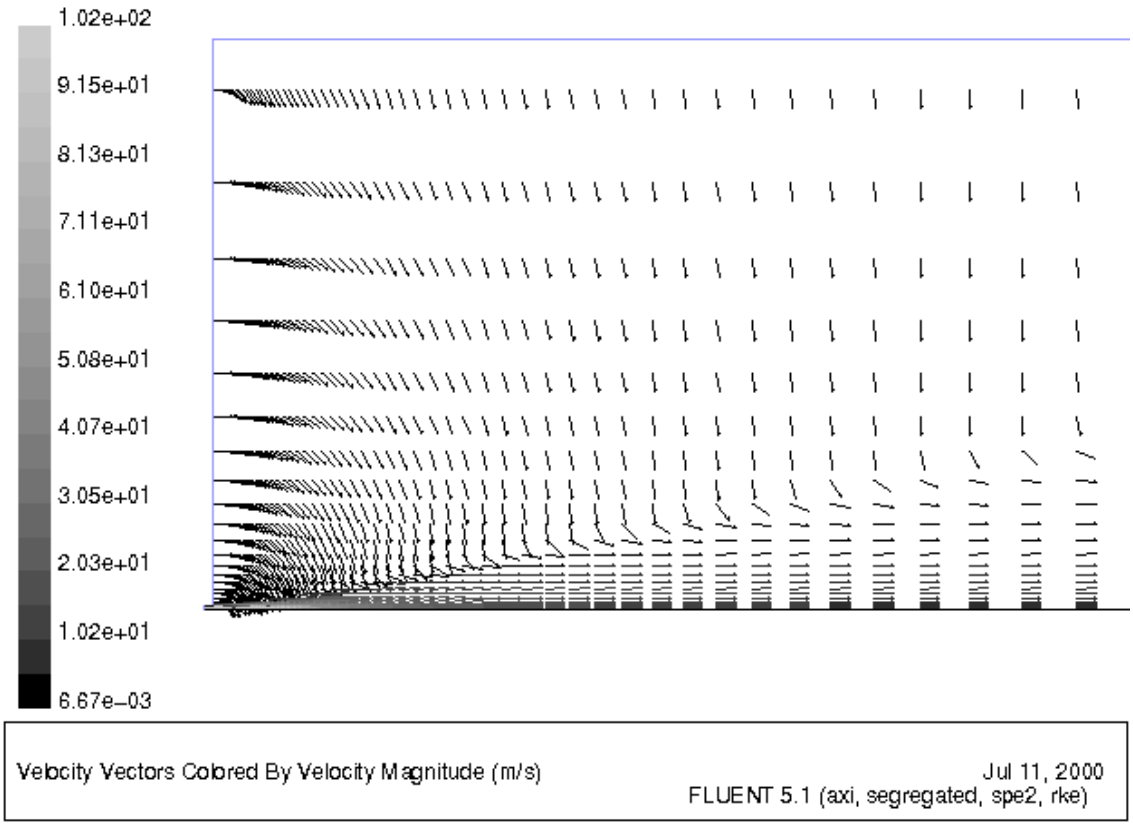


Figure 5: Velocity Vectors for a Free Jet of Silane with the Realizable k-ε model

The results from FLUENT's prediction for a free jet must be compared with generally accepted trends for subsonic, axisymmetric, turbulent free jets expanding into a quiescent atmosphere. Becker, Hottel, and Williams (BHW) analyzed the nozzle fluid concentration for a jet of air released into air. The air originating from the nozzle was marked with oil smoke as a tracer. BHW determined how the concentration along the jet's axis decreased as distance from the nozzle increased from the following data fit:

$$\frac{X_0}{X_C} = 0.0925\frac{x}{r_o} \tag{43}$$

where $X_0$ is the concentration of the source fluid from the nozzle, $X_C$ is the concentration (volume fraction) of the source fluid along the jet's axis, x is the distance from the nozzle, and $r_0$ is the radius of the nozzle (1). Equation (43) is valid when the flow is self-similar. Flow is considered self-similar when one concentration ($X_0$) and one length scale ($r_0$) are sufficient to predict the dimensionless functions ($x/r_0$ and $X_0/X_c$) of one geometrical variable (5).

Assuming that the ideal gas law is applicable, the rate of spread is independent of the source fluid, but the coefficient in equation (43) is not. Since BHW used an air/air jet, the

coefficient of 0.0925 needs to be corrected for silane. To scale the concentration for a compound other than air, the coefficient in Equation (43) must be multiplied by the square root of the ratio of densities for the two compounds (5):

$$\frac{X_0}{X_c} = 0.0925 \frac{x}{r_0} \left( \frac{\rho_a}{\rho_0} \right)^{1/2} \tag{44}$$

where $\rho_0$ is the density of the fluid originating from the jet, and $\rho_a$ is the density of air at ambient conditions. Figure 6 shows how FLUENT's predictions compare with BHW's experimental results and data fit. The maximum offset for the realizable k-ε model was 3.3% and 25% for the standard k-ε model, and the average offset for the realizable k-ε model was 1.0% and 15% for the standard k-ε model.

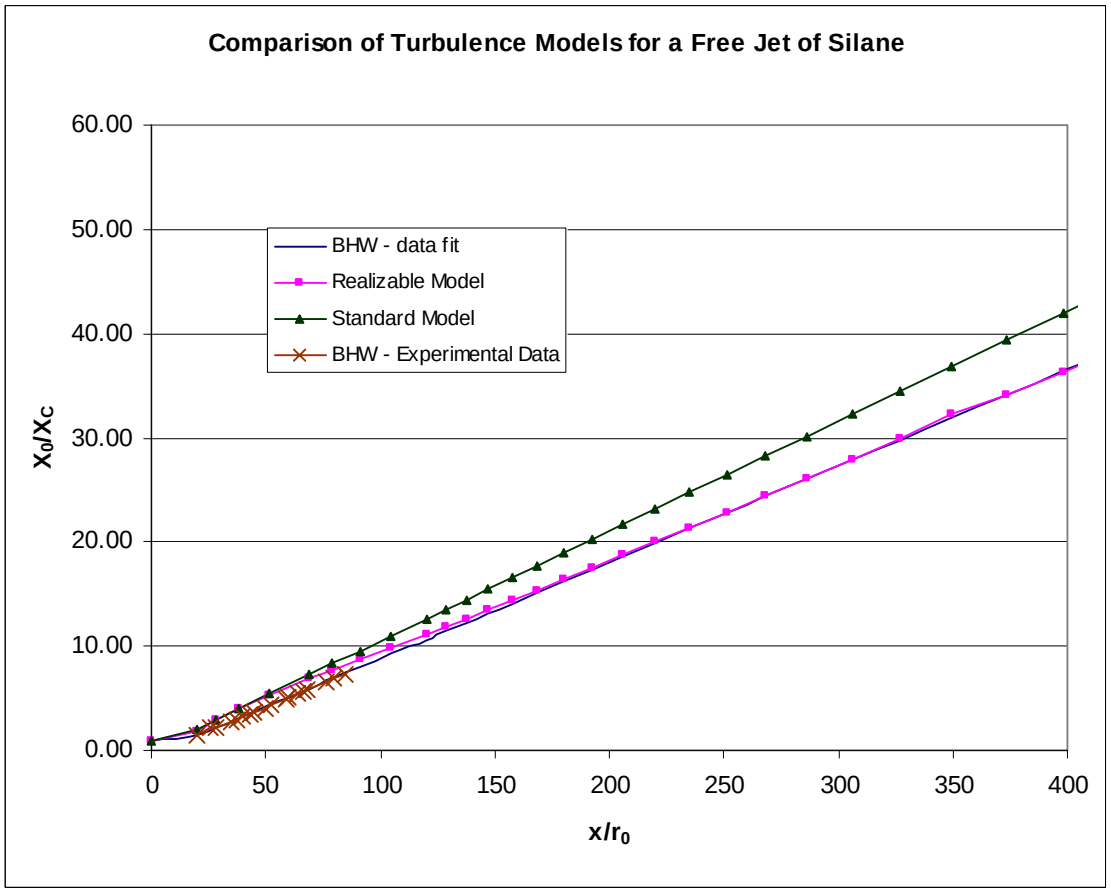


Figure 6: Comparison of the Realizable k-ε Model and Standard k-ε Model with Experimental Data and Data Fit for a Turbulent Free Jet

Self-similarity for the jet of silane is not possible close to the nozzle because of the variation in density across the flow (5). From the Figure 6, self-similarity for the

realizable k-ε model occurs around 150 nozzle radii. Clearly from Figure 6 the realizable k-ε model predicts free jets better than the standard k-ε model especially in the self-similar region. This was actually expected since the realizable k-ε model corrected the "round jet anomaly" from the standard k-ε model. Therefore, FLUENT's realizable turbulence model predicts the jet's centerline concentration to within 3%.

FLUENT can determine the total volume of the silane/air mixture between the UEL and LEL (96 volume% and 1.4 volume%). For an axisymmetric problem, the volume is calculated by rotating the area in Figure 4 around the jet axis from 0 to 2π. The volume of the explosive mixture is calculated by summing the volumes of all the cells between the specified concentrations.

$$V_{mix} = \int dV_{mix} = \sum_{i=1}^{n} |V_i| \tag{44}$$

FLUENT can also calculate the amount of silane in the explosive volume. The volume integral is computed by summing the product of the cell volume by the volume concentration of $SiH_4$ in that cell (9).

$$V_{SiH_4} = \int dV_{SiH_4} = \sum_{i=1}^{n} X_{SiH_4,i} |V_i| \tag{45}$$

Table 5 shows FLUENT's predictions for the total volume of the explosive mixture and the amount of $SiH_4$ within the mixture from both turbulence models compared with the numerical integration of BHW's jet data to determine these volumes (1,14).

Table 5: Comparison of FLUENT's prediction for Volume of the Explosive Mixture and Volume of $SiH_4$ in the Mixture with Numerical Integration of Jet Data

| | $V_{mix}$ ($m^3$) | $V_{SiH4}$ (mL) |
|---|---|---|
| Integration of Jet Data | 0.0310 | 650 |
| Realizable k-ε model | 0.0295 | 621 |
| Standard k-ε model | 0.0243 | 508 |

# Normal Plate-Impinging Jet

## Effect of Plate Distance on Releases of Silane

### Problem Description

Since FLUENT accurately predicted the expansion of an axisymmetric, turbulent jet into stagnant surroundings, the CFD code then was used to simulate a jet impinging on a plate that is normal to the jet. To study the effect of the distance of the plate from the nozzle on the volume of the silane/mixture, the position of the plate was varied between $L/D_{nozzle}$ = 35 (L = 0.160 m) and $L/D_{nozzle}$ = 400 (L = 1.83 m). Equation (44) predicts the

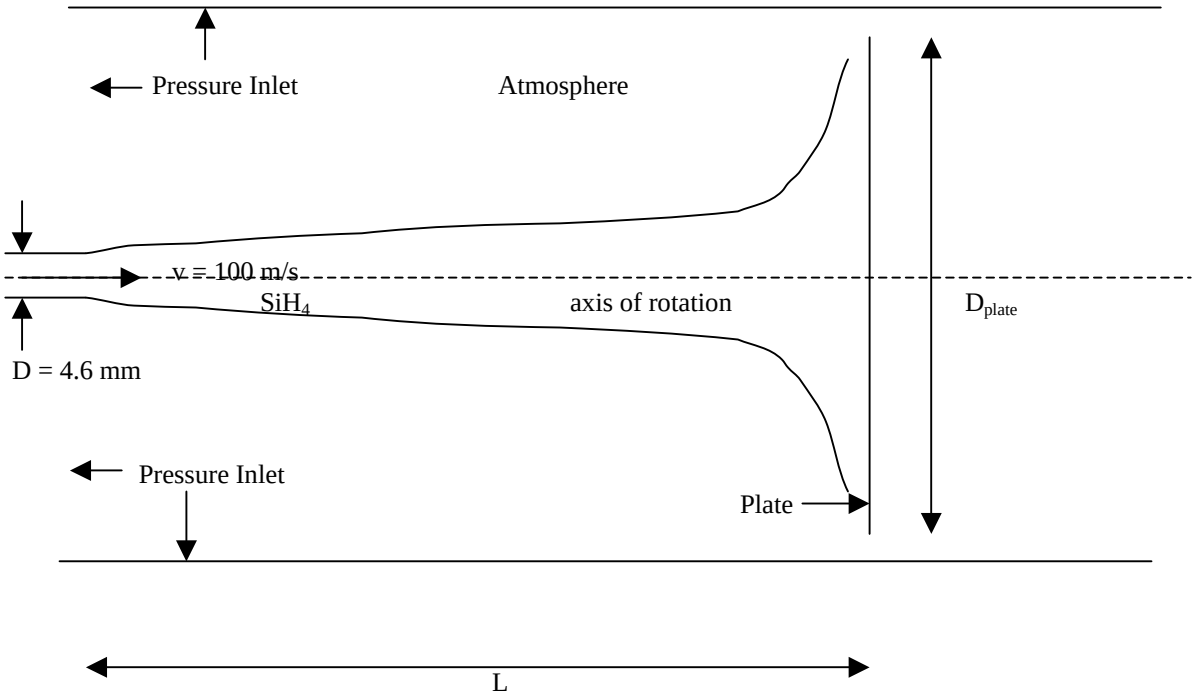


Figure 7: Problem Description for a Plate-Impinging Jet

centerline concentration of 1.4% to occur around 1.71 m, and FLUENT predicts a distance of 1.73 m for a centerline concentration of 1.4 volume%. Therefore, if the jet could fully expand to form the explosive volume, the length of the explosive volume would be about 1.73 m.

Figure 7 shows a schematic of the problem. The diameter of the nozzle, $D_{nozzle}$, is 4.6 mm (0.18 in). The distance of the plate from the nozzle, L, varies. The plate radius is large enough to confine the entire explosive mixture within the plate. Again the boundary of pressure inlet simulated the boundaries of the atmosphere. This problem is also axisymmetric, so only the top half of Figure 7 is modeled with FLUENT.

**Flow Properties and Boundary Conditions**

The material properties listed in Table 1 and Table 2 and the boundary conditions listed in Table 3 are the same for the jet confined by a plate. The realizable k-ε model was used to model turbulence.

**Grid**

Figure 8 shows a typical grid for a jet impinging onto a plate, and Figure 9 shows a close up of a typical grid around the nozzle and the plate. Large gradients in flow occur around the nozzle and the plate. To model these gradients accurately, the nodes of the grid were concentrated along the jet axis around the nozzle and plate. The nodes were also concentrated radially toward the symmetry axis and along the plate. In general, the grid should be densest where jet flow occurs.

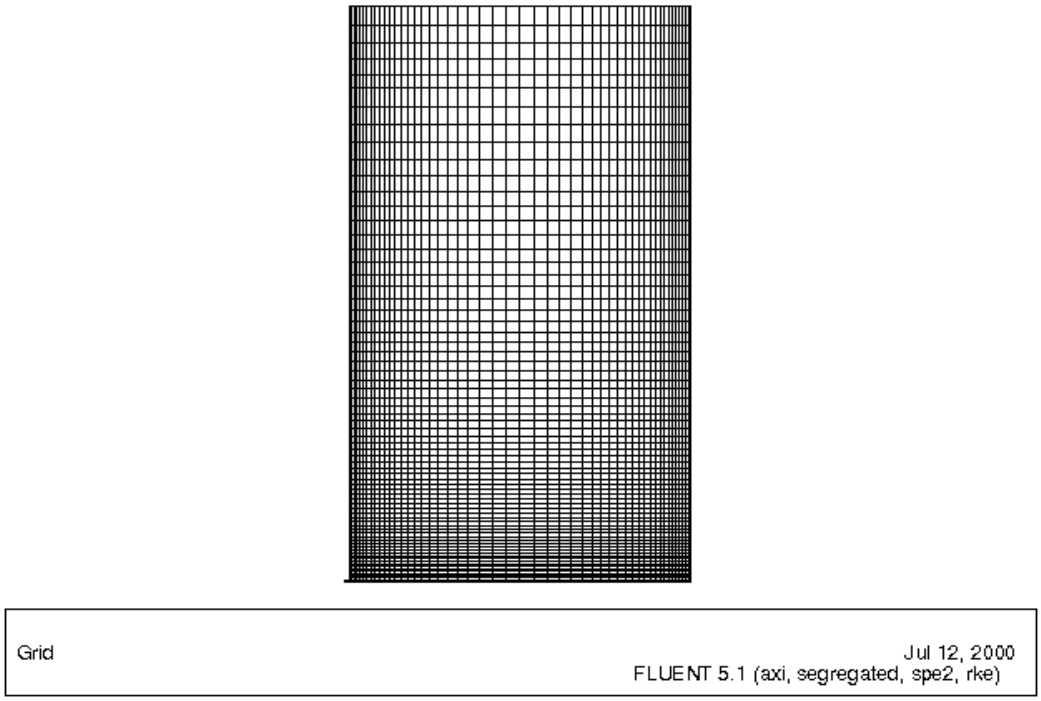


Figure 8: Sample Grid for a Plate-Impinging Jet (for this particular grid L = 0.457 m and $r_{plate}$ = 0.70 m)

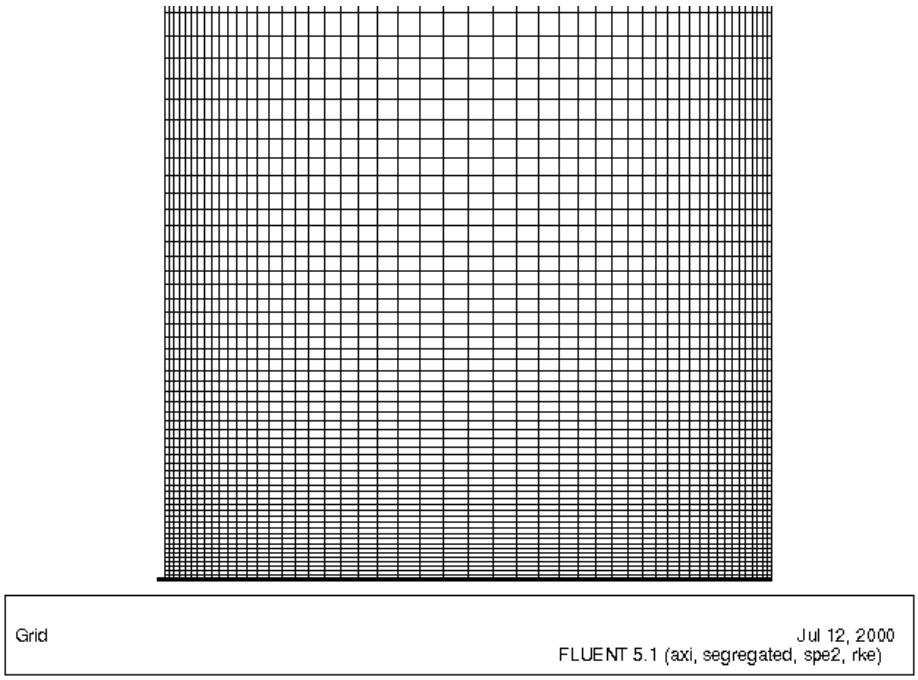


Figure 9: Close up of Grid Near the Jet Axis

**Results**

The jet initially behaves like the free axisymmetric turbulent jet, then it enters a zone near the plate of strong deflection and momentum change in the radial direction (2). Figure 10 shows a close up of the velocity vectors around the nozzle and plate to show the change in direction of flow for a typical plate-impinging problem. Also, the picture shows that air is being entrained into the jet. Figure 11 shows the top profile of the silane/air mixture that forms. Since the problem is axisymmetric the picture must be rotated around the jet centerline to visualize the explosive volume. The concentration of silane is high very close to the nozzle. As the jet entrains air, the silane concentration decreases away from the nozzle.

As the distance of the plate from the nozzle increases, the axial contribution to the volume increases, and the radial contribution decreases. The radial contribution decreases as plate distance increases because the concentration decreases at further distances from the nozzle. Therefore, the location of the concentration of 1.4 volume% silane along the plate decreases as distance increases. Figures 11 to 14 show the effect of plate distance on the volume of the explosive mixture. (Again note that upper concentration in the figures is set at 10% just to show resolution in the volume of the jet.) As these figures indicate, the plate radius required to confine the entire explosive volume within the plate decreases as its distance from the nozzle increases. Figure 15 shows the how the minimum radius to confine the entire explosive volume decreases as the plate location increases.

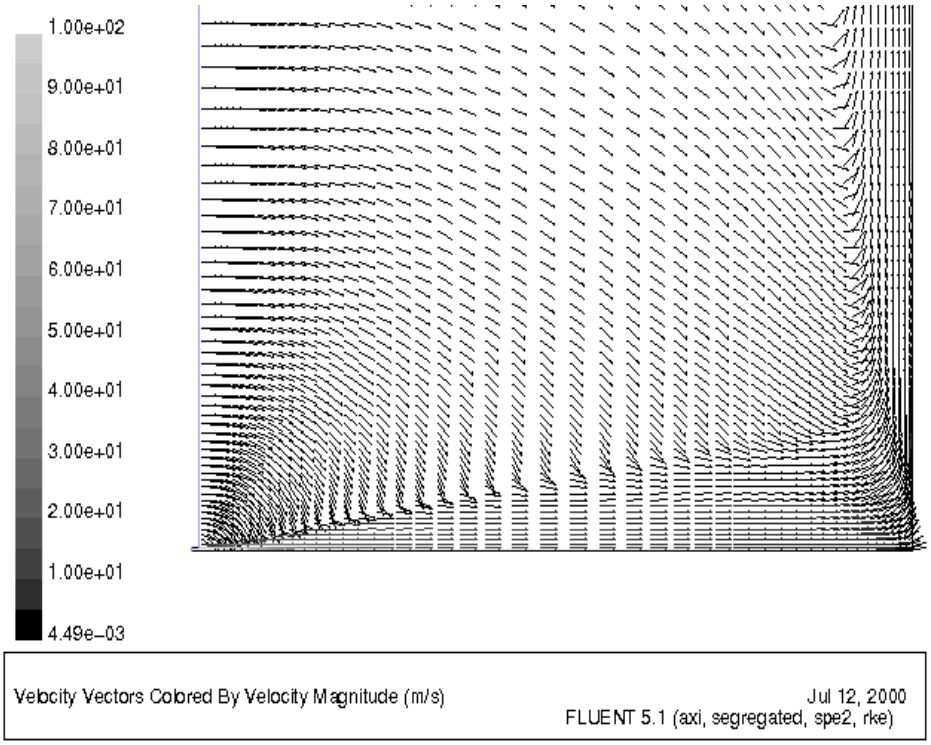


Figure 10: Velocity Vectors for a Sample Plate-Impinging Jet Problem

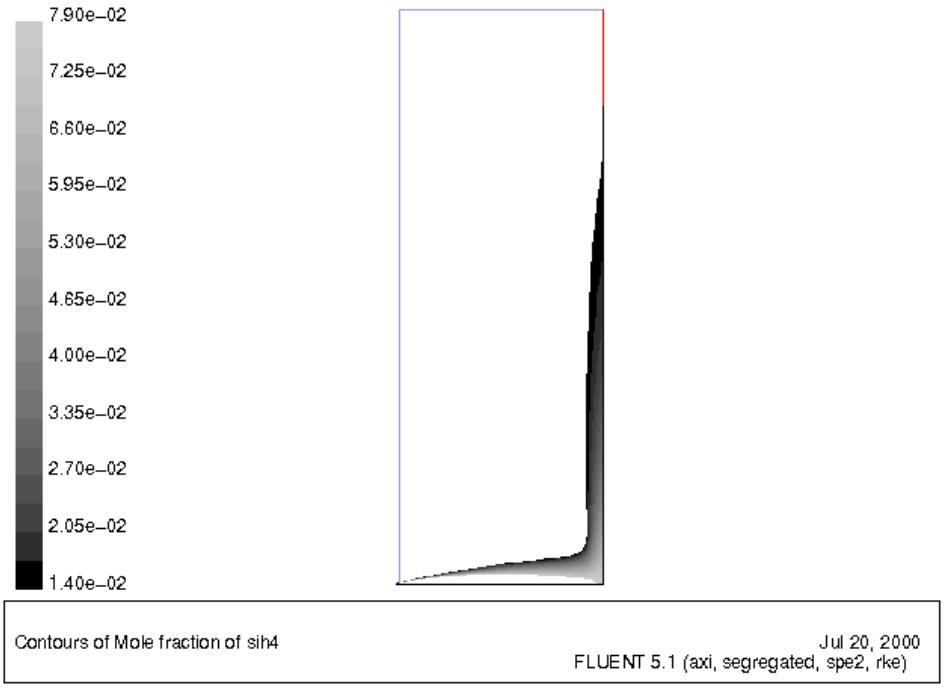


Figure 11: Explosive Volume for a Silane/air Mixture at $L/D_{nozzle}$ = 70 (L = 0.320 m)

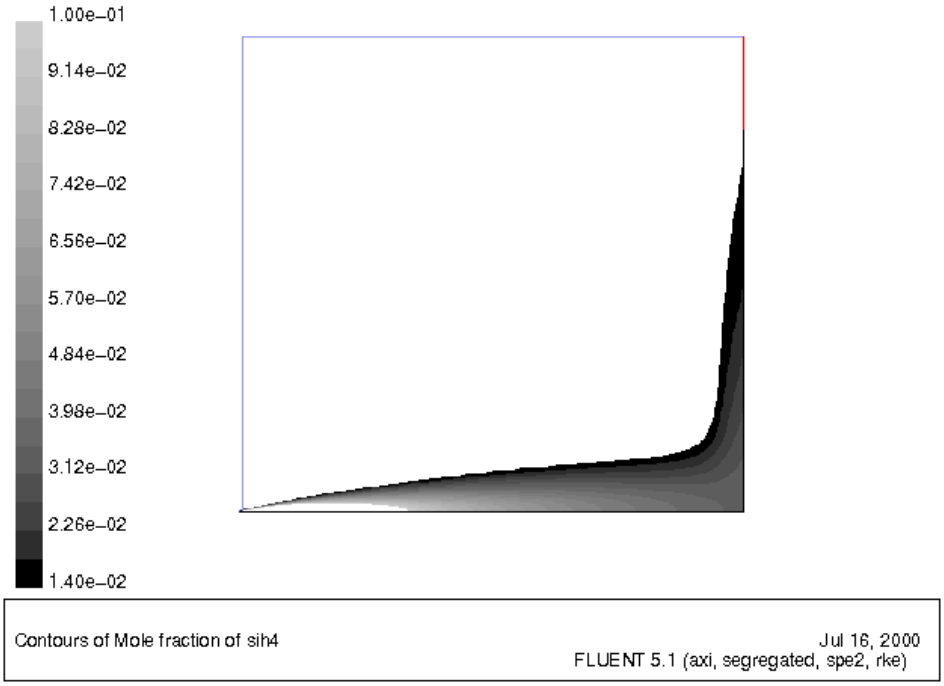


Figure 12: Explosive Volume for a Silane/air Mixture at $L/D_{nozzle}$ = 150 (L = 0.686 m)

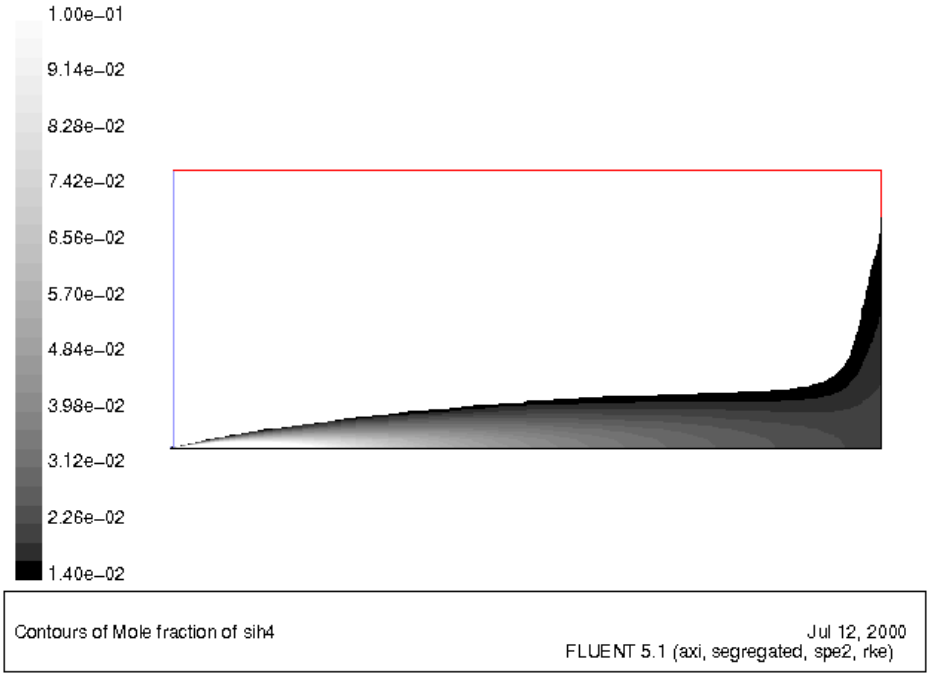


Figure 13: Explosive Volume for $L/D_{nozzle}$ = 250 (L = 1.14 m)

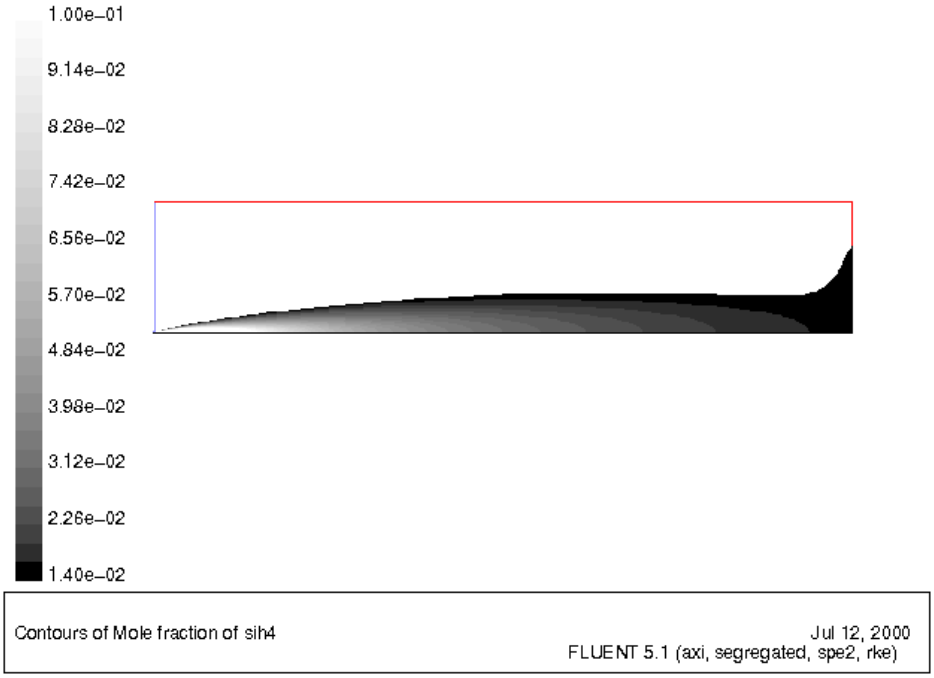


Figure 14: Explosive Volume for $L/D_{nozzle}$ = 350 (L = 1.60 m)

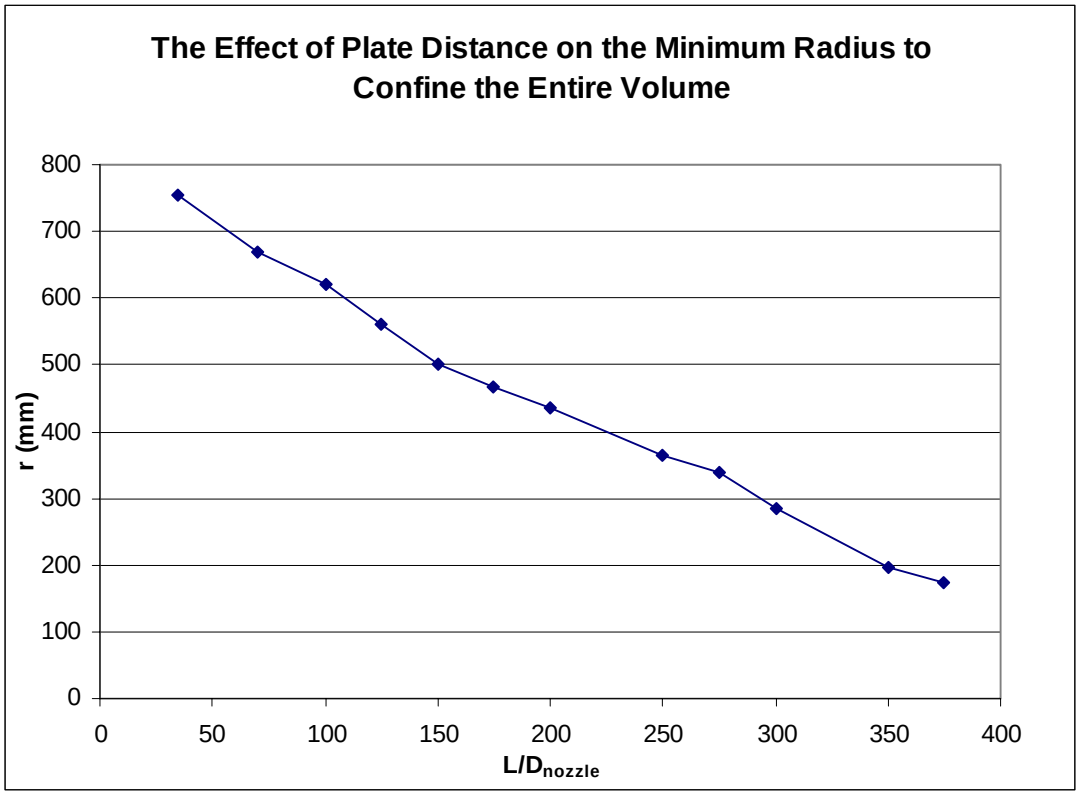


Figure 15: Minimum Radius to Confine the Entire Explosive Volume as Plate Distance Increases

Figures 16 and 17 show how the volumes change with plate distance. When the plate is very close to the nozzle most of the volume is in the radial direction as in Figure 11. Therefore the radial contribution dominates the volume. The volume decreases as plate distance increases when the flow is mostly in the radial direction. As the plate distance increases the axial contribution to the volume increases, so the volume increases as in Figures 13 and 14. In Figures 16 and 17 the volumes go through a minimum around $L/D_{nozzle} = 150$, because neither the radial or axial contribution dominates the volume. Figure 12 shows the volume for $L/D_{nozzle} = 150$. Note that for distances greater than 375 nozzle diameters (L = 1.7145 m) the volumes are no longer affected by the plate (FLUENT predicted the total length of the explosive volume for the unconfined jet to be L = 1.73 m). This can be seen in both figures. In the figures, the total volume and the amount of silane in the total volume at 400 nozzle diameters was equal to the volumes for the unconfined jet expanding into stagnant surrounding. About 300 nozzle diameters downstream from the jet origin, FLUENT predicts a slightly larger total volume and volume of silane than the volumes for the free jet. The reason for the slight increase in volume is probably due to the deflection near the plate. The bulk of the volume is in the free jet part, but near the plate the flow is deflected radially. The conical section of

volume near the plate takes up more space than the small segment of the volume that would be past the plate distance for the unconfined jet.

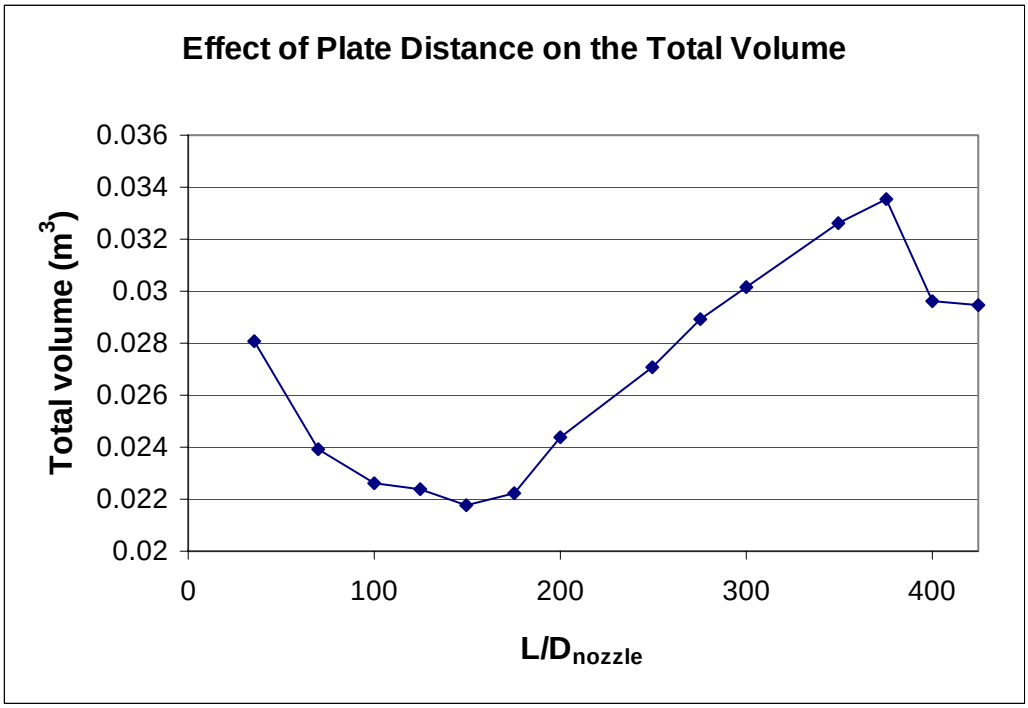


Figure 16: Effect of Plate Distance on the Total Volume

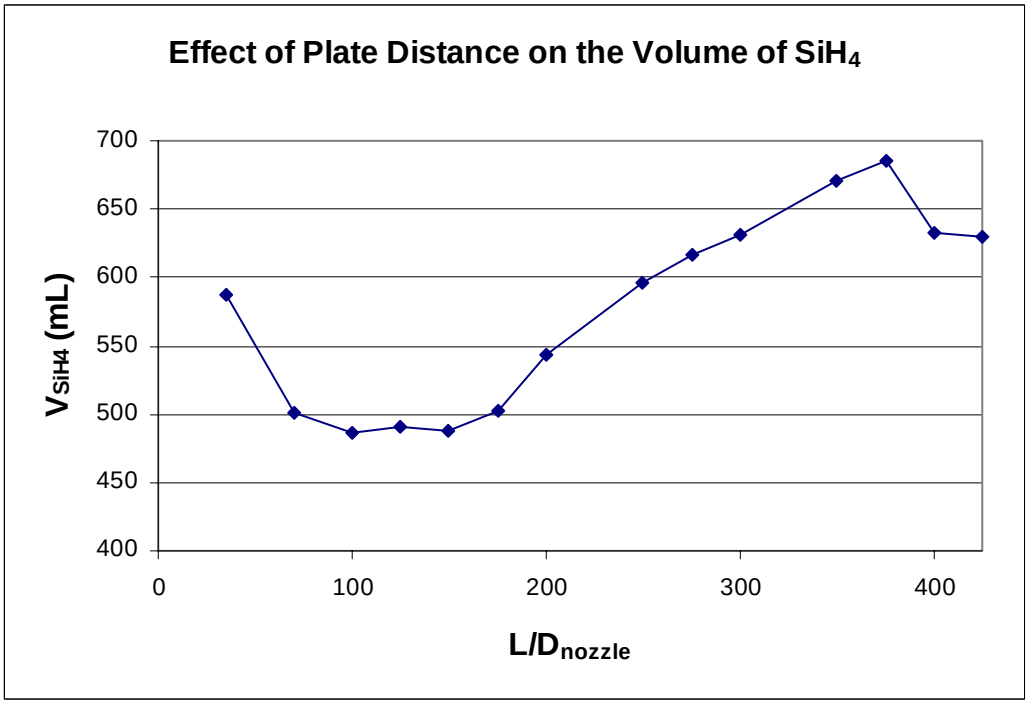

Figure 17: Effect of Plate Distance on the Volume of Silane

## Effect of Plate Radius on Releases of Silane

The preceding section studied the effect of plate distance on the volume, and the entire explosive volume was confined within the plate. This section shows the effect of decreasing the radius at a given plate distance below the minimum diameter that will confine the entire volume. The problem description is the same as Figure 7, and the boundary conditions and fluid properties are the same values, also. Similar weighting factors were used to create the grids. Weighting factors were used to concentrate the grids near the nozzle exit and plate, towards the axis, along the plate, and also above and behind the plate. The grid was dense where jet flow occurs.

### Results

Figures 18 and 19 show the effect of decreasing the plate diameter at 150 nozzle diameters (L = 0.6858 m) downstream from the nozzle. It is evident from both plots that there seems to be four distinct ranges for the plate radius. The first range is from a radius of 0 mm to a radius around 50 mm, the second range occurs between 50 mm to 75 mm, the third is from 75 mm to 500 mm, the final range is the constant volume greater than 500 mm. Each of these ranges will be explained later.

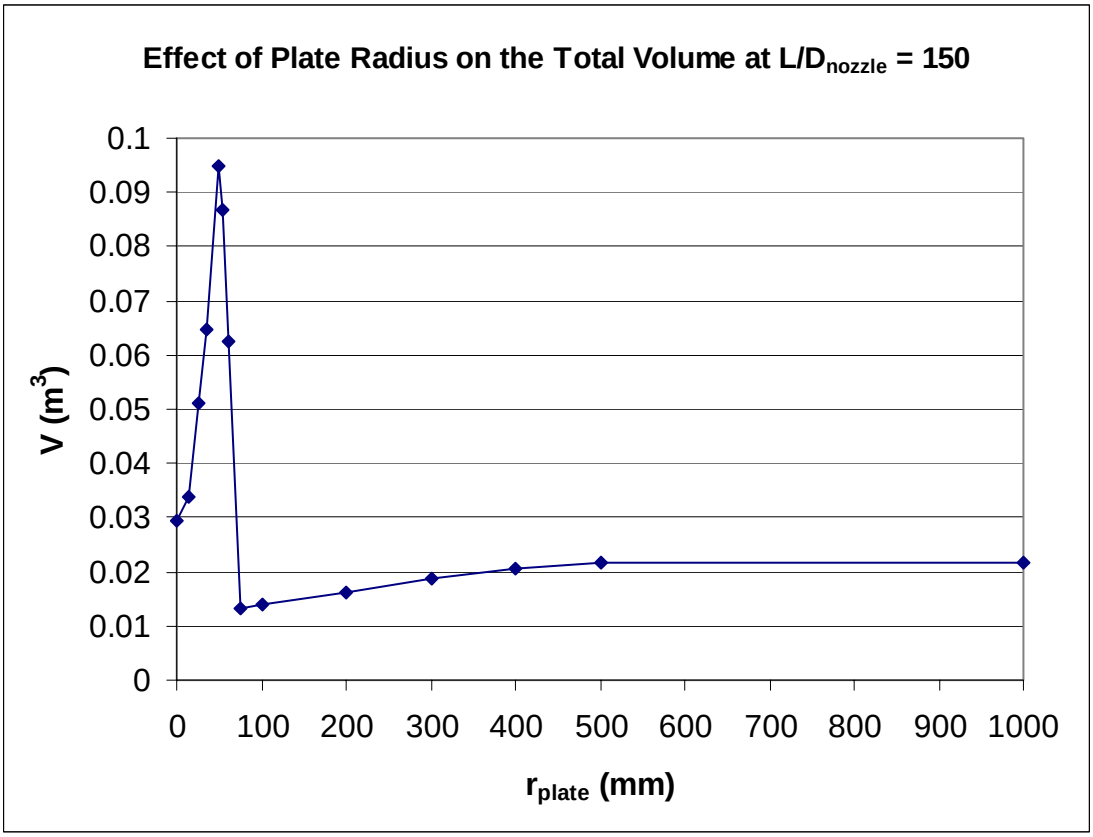


Figure 18: Effect of Plate Radius on the Total Volume at $L/D_{nozzle} = 150$

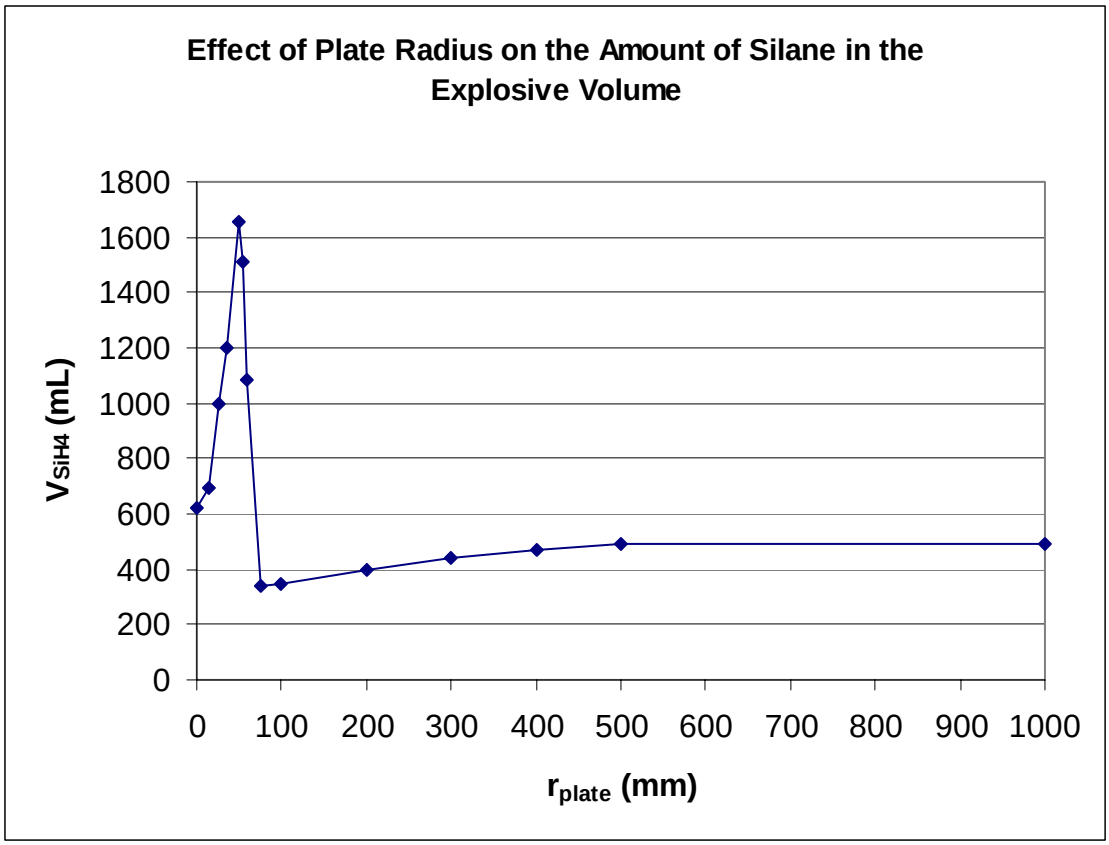


Figure 19: Effect of Plate Radius on the Volume of Silane at $L/D_{nozzle} = 150$

FLUENT predicted a minimum radius to confine the entire explosive volume within the plate at a radius of 502 mm. Therefore, the volumes are constant for any plate radii above this minimum plate radius. The minimum plate radius and the effect of distance on the radius to confine the entire volume were discussed in the preceding section. Figure 12 shows a FLUENT plot with a plate radius of 550 mm at $L/D_{nozzle} = 150$.

As the plate radius decreases the plate no longer confines the entire jet, and the volume fraction of 1.4 volume% is now past the plate's edge. The jet's momentum is still in the radial direction past the plate's edge. Figures 18 and 19 show the volumes decrease fairly linearly as the plate's radius decreases until 75 mm. The volume decreases because the plate no longer blocks air from being entrained into the mixture from behind the plate. As the plate diameter decreases the jet can entrain air sooner into the mixture and dilute it, so the volume will decrease as the diameter of the plate decreases. Figures 20 and 21 show examples of plate radii that do not confine the entire explosive within the plate. They also show that the volume decreases as the plate radius decreases.

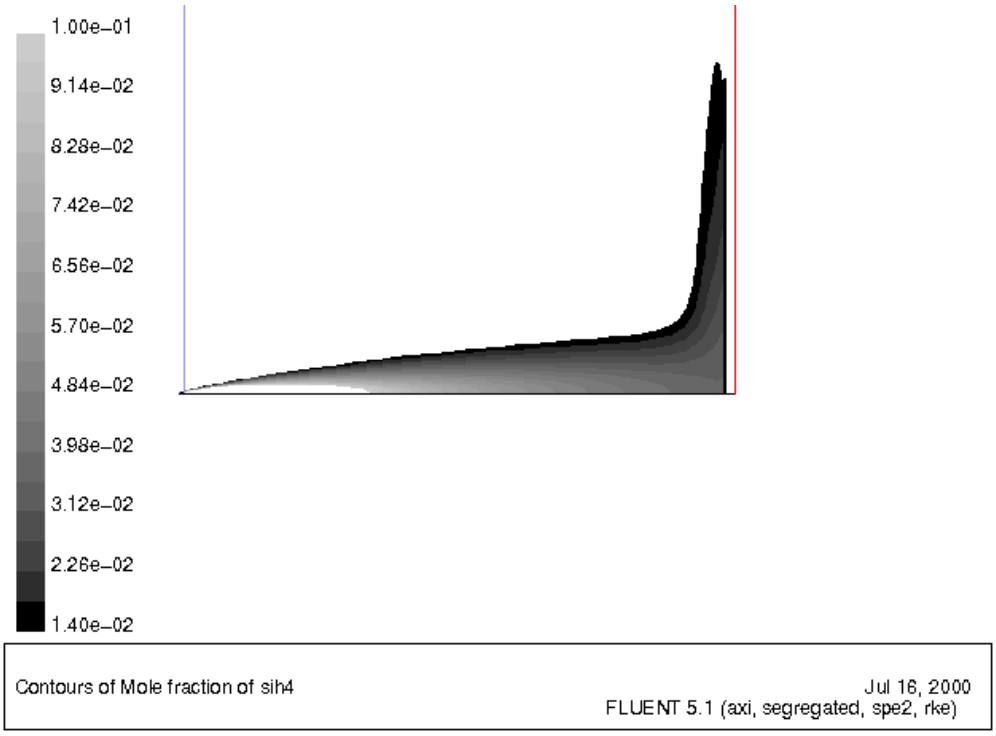


Figure 20: Explosive Volume for $L/D_{nozzle}$ = 150 and $r_{plate}$ = 400 mm

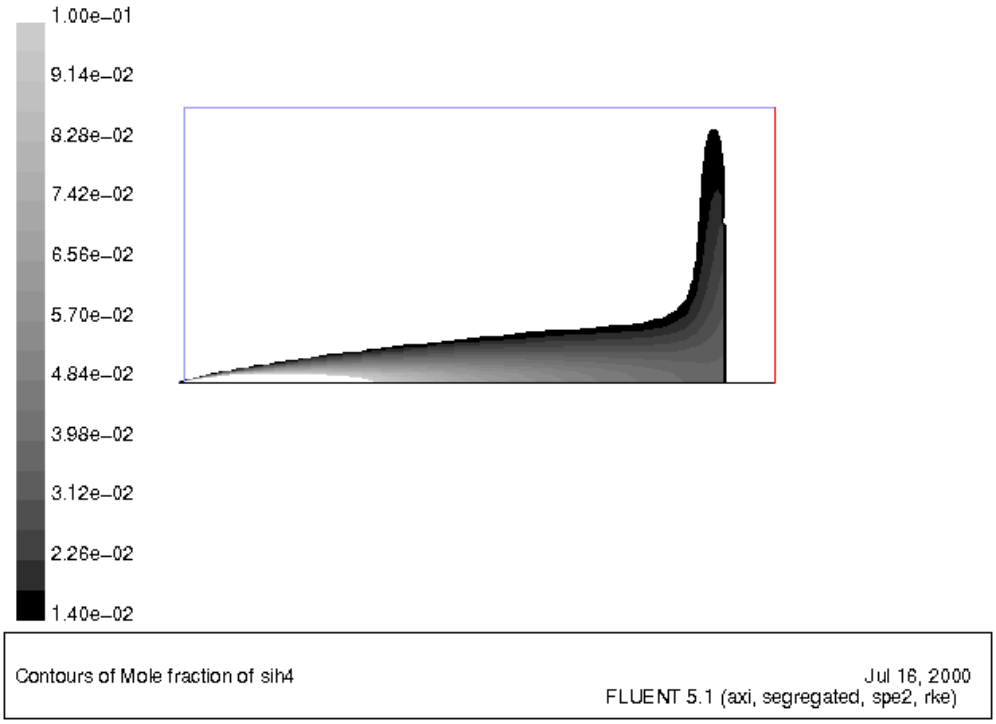


Figure 21: Explosive Volume for $L/D_{nozzle}$ = 150 and $r_{plate}$ = 200 mm

The volumes decrease when the plate radius decreases until the plate radius is approximately the width of the jet at 1.4 volume%, which is about 75 mm. At 75 mm a vortex develops behind the plate, and if the vortex is wide the jet cannot flow past the vortex. As the plate radius decreases the vortex also decreases, and the jet can flow past the vortex. Figure 22 shows the velocity vectors for a radius approximately equal to the jet width, and part of the vortex that develops behind the plate. Figures 23 and 24 show how the volume between the flammable limits for a silane/air mixture sharply increases due to the decrease in plate radius and size of the vortex. Also, note that jet flow is not just in the radial direction near the plate. As the plate diameter decreases, the jet flows in the radial and axial direction past the plate.

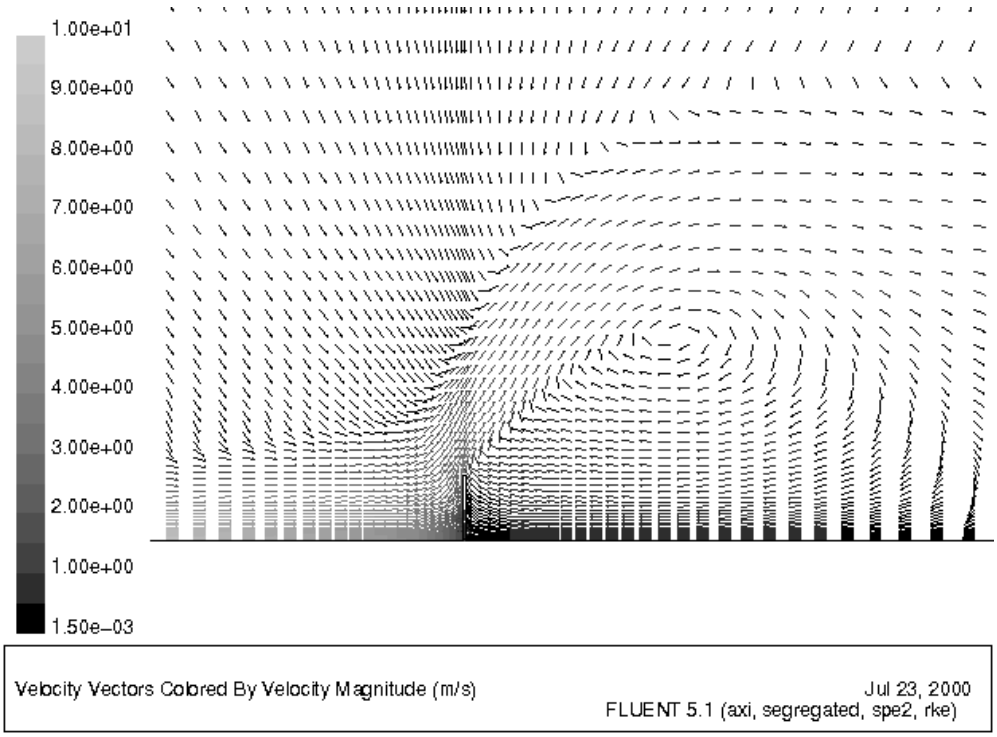


Figure 22: Velocity Vectors for $L/D_{nozzle} = 150$ and $r_{plate} = 60$ mm

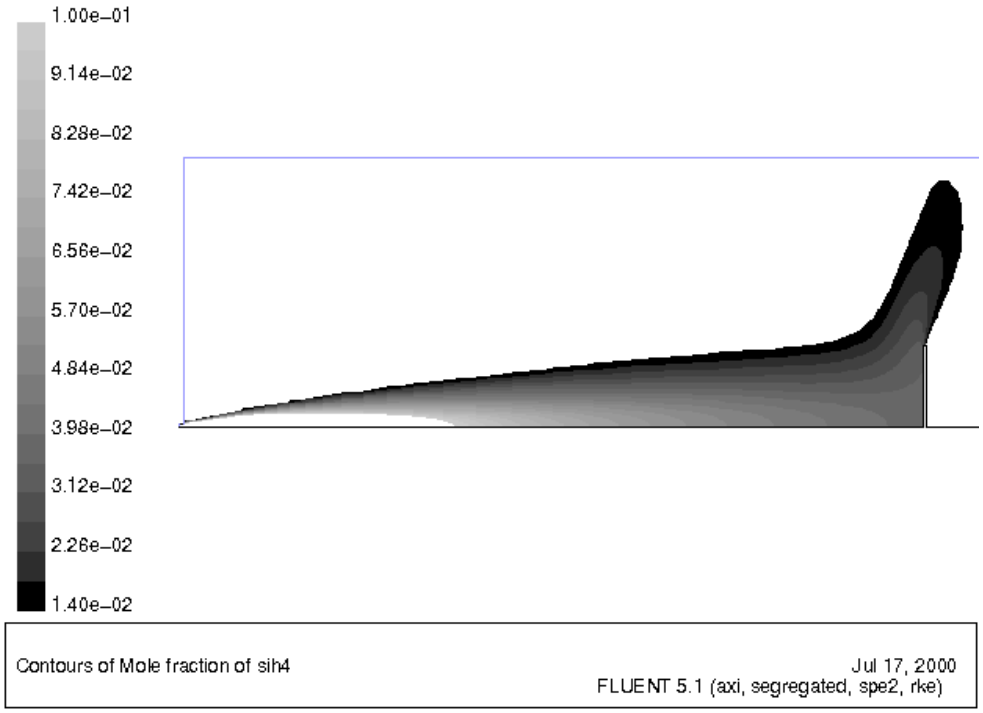


Figure 23: Explosive volume for $L/D_{nozzle}$ = 150 and $r_{plate}$ = 75 mm

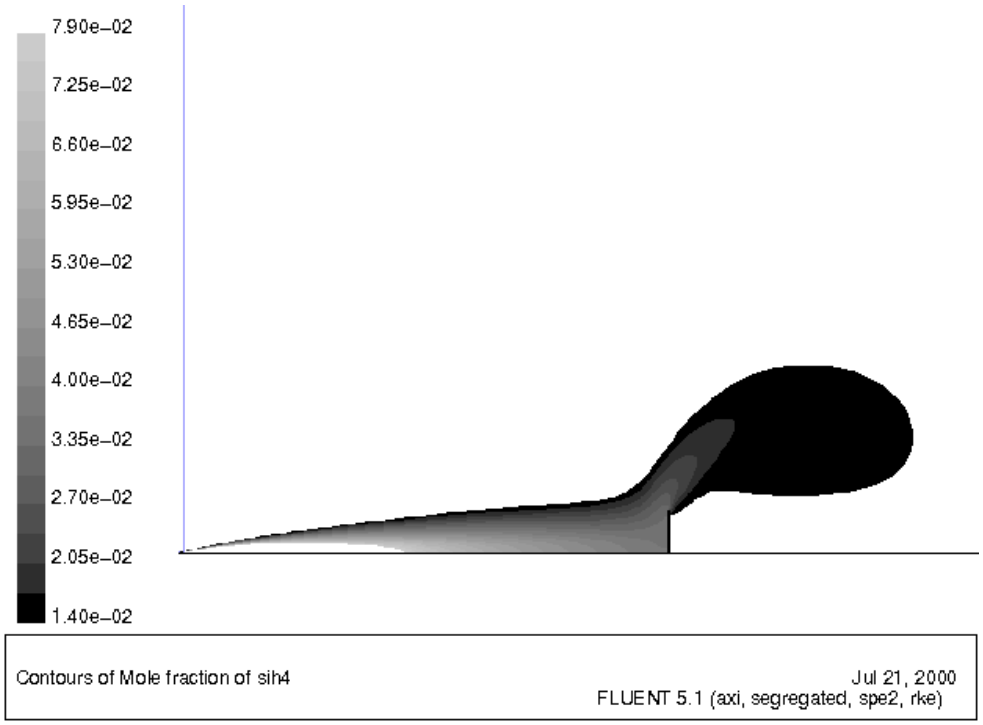


Figure 24: Explosive Volume $L/D_{nozzle}$ = 150 and $r_{plate}$ = 60 mm

The large spike in Figures 18 and 19 occurs when the plate radius is much less than the jet width at 1.4 volume%. The jet just flows past the plate. A vortex still develops behind the plate, but the vortex is small enough that the jet can flow past it. However, the plate and the vortex cause the jet to widen, which increases the flammable volume. As the plate diameter decreases, the vortex decreases so the jet is not so wide, which decreases the flammable volume. Eventually the diameter of the plate will be so small that it no longer affects the jet, and the volume between the UEL and LEL approaches the volume for a free jet. Figure 25 shows the velocity vectors for a plate radius of 35 mm at $L/D_{nozzle}$ = 150. It is evident from the picture that vortex behind the plate is much smaller, and the jet flows over the vortex. Figures 26 and 27 are the profiles of the flammable volumes at radii of 35 mm and 25 mm. Note that the width of the volume is smaller due to the smaller plate size and vortex.

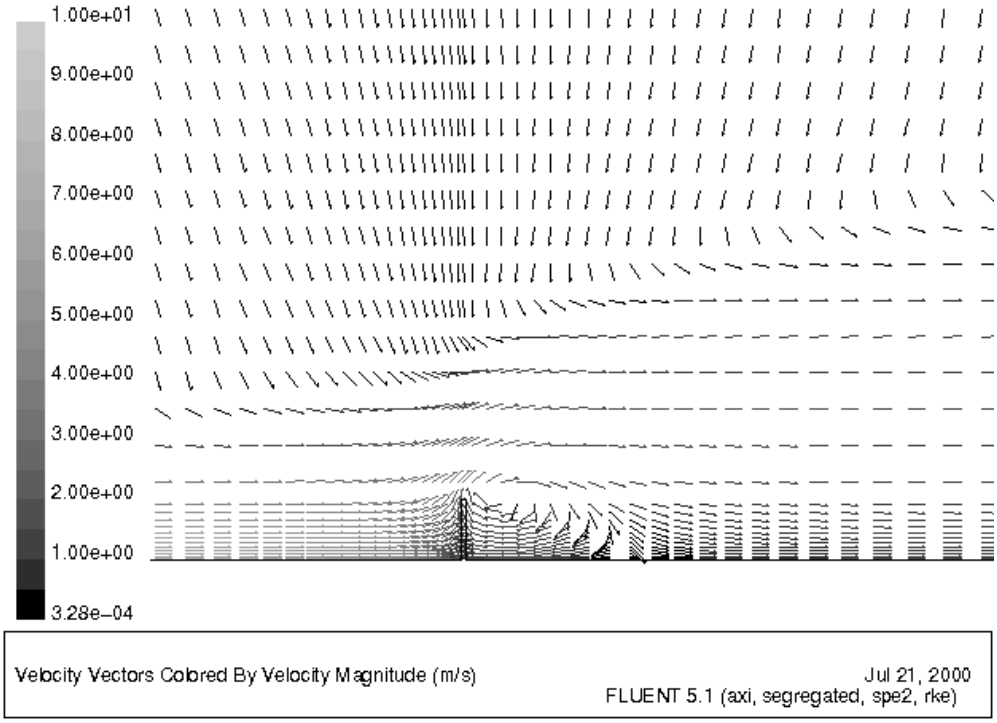


Figure 25: Velocity Vectors for $L/D_{nozzle}$ = 150 and $r_{plate}$ = 35 mm

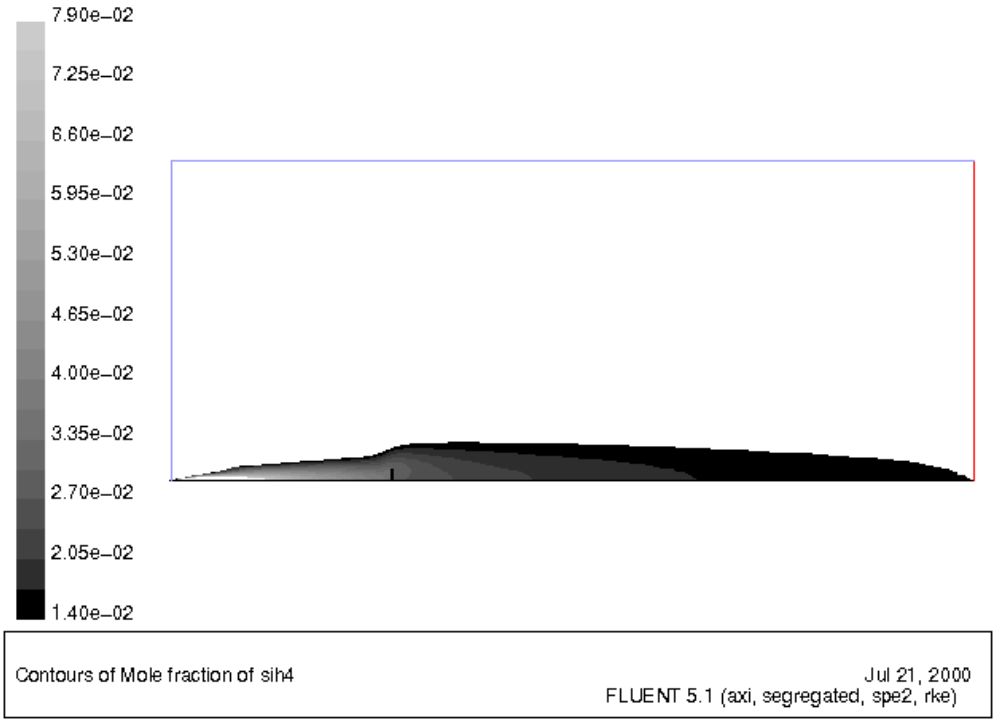


Figure 26: Explosive Volume at $L/D_{nozzle}$ = 150 and $r_{plate}$ = 35 mm

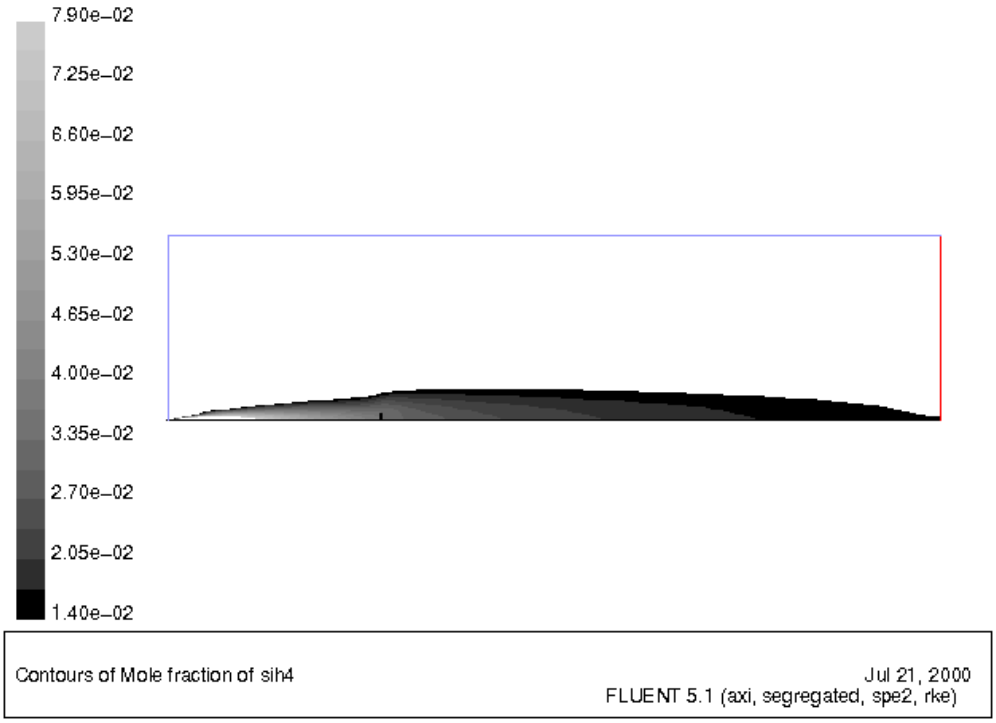


Figure 27: Explosive Volume for $L/D_{nozzle}$ =150 and $r_{plate}$ = 25 mm

## Conclusions and Future Work

The realizable k-ε turbulence in FLUENT predicts the axisymmetric, turbulent free jets accurately. The realizable k-ε turbulence model therefore can be used to predict trends for plate impingement for a round turbulent jet.

The volume between the UEL and LEL and the amount of silane in the total volume are a function of plate radius and plate location. The volumes decrease with increasing plate distance when the radial contribution dominates, and the volumes increase with increasing plate distance when the axial contribution dominates. The radius that confines the entire volume decreases as the plate distance increases. The volumes increase, decrease, or remain constant depending on the diameter of the plate.

Future work includes normalizing the data for the plate-impinging jet, and developing generalized correlations for any plate radius at any plate location. In the near future, FLUENT will be used to model more complex 3D flow like flow past a cylinder. Past a cylinder, the flow is no longer axisymmetric but a function of the cylinder's distance, radius, and height. (In FLUENT, the cylinder will be long enough so the jet won't flow past the top and bottom of the cylinder). Generalized correlations will be developed for flow past a cylinder for any cylinder radius and location.

**References:**


1. Becker, H. A., Hottel, H. C., Williams, G. C.; "The Nozzle-Fluid Concentration of the Round, Turbulent, Free Jet," Journal of Fluid Mechanics, 1967 Vol. 30 part 2 pp 285 – 303

2. Becker, H. A., Cho, S. H., Ozum, B., Tsujikawa, H.; "Turbulent Mixing in the Impingement Zone of Dual Opposed Free Jets and of the Normal Wall-Impinging Jet," Chemical Engineering Communication, 1988 Vol. 67 pp 291 - 313

3. Bird, R. B.; Stewart, W. E., and Lightfoot, E. N.; Transport Phenomena 1960

4. Britton, L. G.; "Combustion Hazards of Silane and Its Chlorides," Plant/Operations Progress, January 1990, Vol. 9, no. 1 pp 16 - 38

5. Chen, C. J. and Rodi, W., Vertical Turbulent Buoyant Jets – A Review of Experimental Data, 1980

6. Chowdhury, N.; "Silane Safety Study: Compressed Gas Association Performs Large Scale Tests," Semiconductor Safety Association, Winter 1997, pp 47- 57

7. Cruice, W.; "Effects of Releases of Silane Mixtures in Ambient Air," HRC Report 4007, December 15, 1978

8. Cruice, W.; "Leakage of Silane in Cabinets and Ducts," HRC Report 5038, May 11, 1982

9. FLUENT User's Guide Ch. 6, 7, 8, 9, 11, and 21; Fluent Inc. 1998

10. Fthenakis, V. M. and Moskowitz, P. D.; "An Assessment of Silane Hazards," Solid State Technology, January 1990, pp 81 -85

11. Roiglestad, T., Mosovsky, J. Valdes, J. Lichtenwalner, C. P.; "Silane Safety Improvement Project S71 Final Report," SEMATECH Technology Transfer 94062405A-Eng, June 1994

12. Tamanini, F., Chaffee, J. L. and Jambor, R. L.; "Reactivity and Ignition Characteristics of Silane/Air Mixtures," Process Safety Progress, Winter 1998, Vol. 17 No. 4 pp 243 - 258

13. Tamanini, F. and Braga, A.; "A New Perspective on the Behavior of Silane Leaks in Ventilated Enclosures – Implications for the Design of Protection Measures," Semiconductor Safety Association, Winter 1997, pp 21-36

14. Tamanini, F. and Chaffee, J.; "Ignition Characteristics of Releases of 100% Silane," SEMATECH Technology Transfer 9601367A-Eng, March 1996

15. Visokey, M. Tamanini, F. and Chaffee, J. L.; "Effects of Leak Size and Geometry on Releases of 100% Silane," SEMATECH Technology Transfer 96083168A-Eng, September, 1996